CHAPTER 2

Dynamics Modeling of the Space Tether

This chapter is devoted to the dynamics modeling of the TSRS. The dynamics modeling is always the steadfast foundation of any research, and this holds true for the research of the space tethered system. At this point, because space experiments and ground tests are expensive and physically challenging, theoretical research has taken on an important role. Take, for instance, the flexible and elastic tether. It is a difficult feature to study while, on the ground; and it is even more complicated to study in space. Researchers have been dedicated to finding a perfect dynamics model for space tether for decades. However, they still have not come up with a perfect result in their research. If the model is very close to the real physical model, the analysis and numerical computation will be very complex; if the computation efficiency is on the top of the list, the dynamics model cannot describe all the specifics of the physical model. For this reason, there needs to be a trade-off between the reality and the feasibility of the space tethered system. Therefore, we introduce five different dynamics models of the TSRS.

The TSRS is new application for the space tether for short distances. The dynamics of TSRS should be based on the traditional dynamics model of space tether system. Here are five different dynamics models that have been proposed to describe and solve the problem:

(1) The control scheme is designed based on a dynamics model by treating the tether as massless flexible links. A. Misra and P. Williams have used this model to analyze the in-plane and out-of-plane oscillations during the deployment and retrieval via space tether, and designed some different control strategies for these two process [1–5].

(2) A Bead model is derived by treating the flexible tether as a serial of mass points, which are composed by a spring and a damper [6]. Based on the Bead model, Banerjee et al. refined the model. Dynamics and kinetics of the deployment and retrieval of tether are analyzed through changeable mass of bead and length of links [7–9].

Tethered Space Robot
https://doi.org/10.1016/B978-0-12-812309-6.00002-6

(3) The dynamics model of flexible tether and mechanics of the capstan release device are derived based on the Hamiltonian theory. Then, the deployment of the space tethered system can be numerically simulated based on discrete equations by employing the Ritz method [10–12].

(4) The infinitesimal analysis and Lagragian method are employed for modeling dynamics, and the Galerkin method is used for discrete and solving. This method can avoid the complex inherent force analysis of the space tether, and the smart second-order motion equations for the dynamics. While, the equations derived from this method are generally too complicated to analyze, they are strongly coupled with each other [12–14].

(5) A finite element method is utilized to solve the discrete equations of model dynamics derived from the Newton-Euler method [15–19].

In the previous five methods, the model of massless links is too simple to describe the characteristics of TSRS. Although the Ritz method and the Galerkin method are efficient for computation, their accuracy is not guaranteed due to the man-made global modal function. The finite element method is extremely precise to the real model and is considered to be a promising method to solve tether issues, even though it is rather complicated and unstable. As a classic dynamics model for space tether, the Bead model is widely used due to its simple derivation and stable computation in the deployment and retrieval phase in the face of its low computational speed.

This chapter is devoted to the Bead model, Newton-Euler, and Hamiltonian method of the TSR System, which is shown in Fig. 2.1, and is composed of a base satellite (platform satellite), multi degree arm, and manipulator.

The platform satellite and the terminal capture device shown in Fig. 2.1 can be treated as rigid bodies, which are relatively simple due to the classic mechanics of a rigid body. Because the order of size is considerably small compared to the length of tether, the platform satellite and the terminal capture device can be assumed to be mass points. According to the evident characteristics of flexibility and extremely long length (form dozens of meters to several kilometers), the dynamics model of the space tether is relatively complex. To describe the spatial motions of tether, a natural coordinate named s is introduced, which denotes the tether length from an arbitrary elemental mass to a certain terminal endpoint of tether. We define the endpoint of tether from the platform satellite as the beginning of calculation, $\xi(t)$ as the natural coordinate of tether at the connection point between platform and tether, and L as the natural coordinate at the terminal capture device, namely the total natural length of tether.

2.1 DYNAMICS MODELING AND SOLVING BASED ON THE BEAD MODEL

The space tether is divided into discrete systems, and each element is composed of mass point and massless elastic rigid links. As shown in Fig. 2.1, the deployed tether ($s \in [\xi, L]$) is divided into $n+1$ segments, and a mass point is at the end of each segment instead of the mass of this segment. Each segment of tether is simplified as a massless elastic rigid link. The adjacent links are connected by a hinge connection.

A platform coordinate system is introduced to describe the motion of each mass point of the Bead. As expressed in Fig. 2.2 the origin of this coordinate is at the center of mass of the platform satellite, and this coordinate system x-y-z has the x-axis along the tangential of orbit toward motion direction of the platform satellite, z-axis inward from the platform to the Earth along the local vertical, and y-axis along the orbit abnormal completing the right-hand triad. When the motion orbit is assumed to be a circle orbit, mass points in the platform coordinate system are satisfied with C-W equations:

$$\begin{cases} \ddot{x} - 2\omega\dot{z} = a_{mx} \\ \ddot{y} + \omega^2 y = a_{my} \\ \ddot{z} + 2\omega\dot{x} - 3\omega^2 z = a_{mz} \end{cases} \tag{2.1}$$

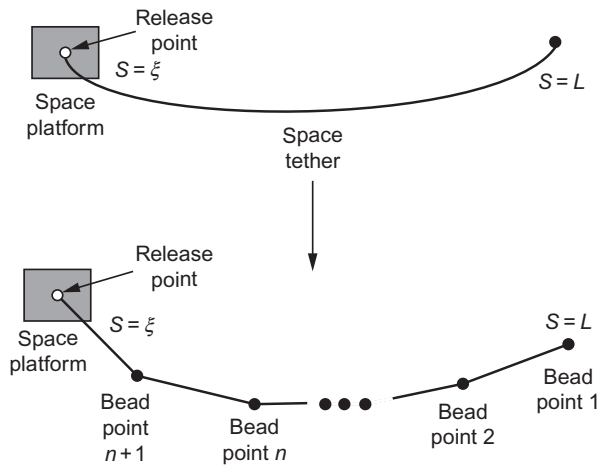

Fig. 2.1 Configuration of Bead model.

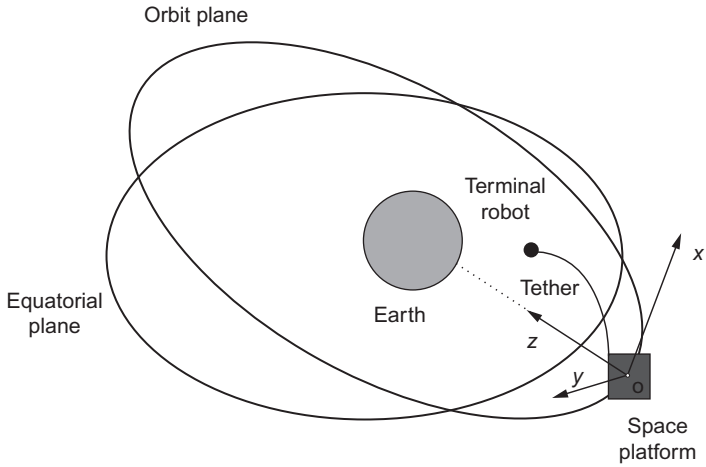

Fig. 2.2 Coordinate system of a platform satellite.

where a_{mx}, a_{my}, and a_{mz} denote the projection of acceleration $\boldsymbol{a}_m$ due to external forces except universal gravitation; ω is orbital angular velocity of platform.

Because the platform satellite is much heavier than the tether and terminal capture device, the effects from the motions of the tether and capture device are ignored, and the center of mass of the system is assumed to be at the center of mass of the platform satellite. Furthermore, to simplify the system, a circular Keplerian reference orbit for the center of mass of the system is assumed. The length of the tether is constant when the Space Tethered Robot is in the station-keeping phase. In this case, the tether can be divided into $n+1$ segments as shown in Fig. 2.1, and the natural length of each segment is l. The motion of each mass point can be derived as:

$$\begin{cases} m_i(\ddot{x}_i - 2\omega\dot{z}_i) = F^x_{i-1,i} + F^x_{i+1,i} \\ m_i(\ddot{y}_i - \omega^2 y_i) = F^y_{i-1,i} + F^y_{i+1,i} \quad (i = 1,2,\ldots,n+1) \\ m_i(\ddot{z}_i + 2\omega\dot{x}_i - 3\omega^2 z_i) = F^y_{i-1,i} + F^y_{i+1,i} \end{cases} \tag{2.2}$$

where $\boldsymbol{F}_{i-1,i}$ is the force on mass point i from $i-1$; $F^x_{i-1,i}$, $F^y_{i-1,i}$, and $F^z_{i-1,i}$ denote the projection of $\boldsymbol{F}_{i-1,i}$ in platform coordinate system; $F^x_{0,1}$, $F^y_{0,1}$, and $F^z_{0,1}$ are constant zeros; and $F^x_{n+1,n+2}$, $F^y_{n+1,n+2}$, and $F^z_{n+1,n+2}$ are the forces from platform. The elastic force in massless elastic rigid link meets the Hook's law:

$$\boldsymbol{F}_{i+1,i} = -\boldsymbol{F}_{i,i+1} = EA\left(\frac{|\boldsymbol{r}_{i+1,i}|}{l} - 1\right)\frac{\boldsymbol{r}_{i+1,i}}{|\boldsymbol{r}_{i+1,i}|} \quad (i = 1, 2, \ldots, n)$$

where $\boldsymbol{r}_{i+1,i} = (x_{i+1} - x_i, y_{i+1} - y_i, z_{i+1} - z_i)^T$, $|r_{i+1,i}|$ denotes the module of $r_{i+1,i}$, E denotes Young's Modulus of the tether, and A is cross-section area of tether. m_i is the mass of each mass point, which is defined as:

$$m_i = \begin{cases} \dfrac{\rho l}{2} + M & i = 1 \\ \rho l & i = 2, 3, \ldots, n+1 \end{cases}$$

The motion of TSRS is solved by using the four-order Runge-Kutta numerical integration of Eq. (2.2).

In the deployment phase, due to the changeable length of tether, the method mentioned above for a constant tether should be improved. To simulate the deployment of the tether, the $n+1$th bead is defined as an anchor. During deployment, the natural length η between the anchor and release point lengthens continuously, while the natural lengths l of other segments are constant, which is shown in Fig. 2.3. However, as the growing of η, the error of simulation increases sharply. To solve this, it is defined that a new element (anchor and link) grows up from the old anchor segment when $\eta \geq 1.5h$, as shown in Fig. 2.4. Then the C-W formula is expressed as:

$$\begin{cases} m_i(\ddot{x}_i - 2\omega\dot{z}_i) = F^x_{i-1,i} + F^x_{i+1,i} \\ m_i(\ddot{y}_i + \omega^2 y_i) = F^y_{i-1,i} + F^y_{i+1,i} \quad (i = 1, 2, \ldots n) \\ m_i(\ddot{z}_i + 2\omega\dot{x}_i - 3\omega^2 z_i) = F^z_{i-1,i} + F^z_{i+1,i} \end{cases} \tag{2.3}$$

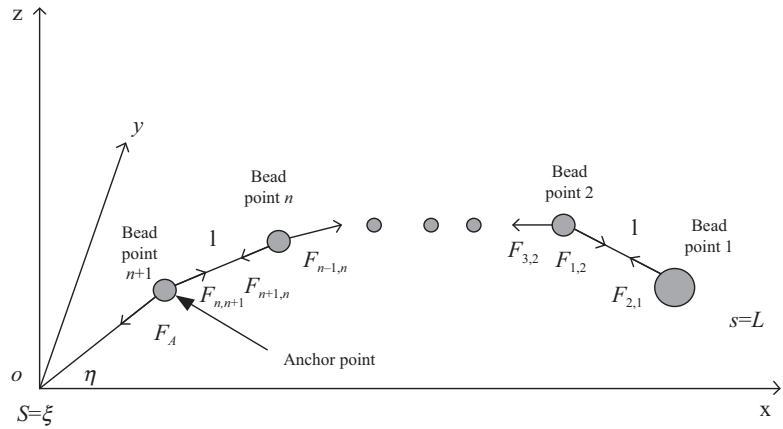

Fig. 2.3 Bead model in a platform coordinate system.

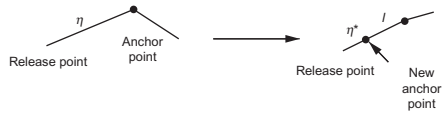

Fig. 2.4 Increase of bead.

The motion of anchor point is:

$$\begin{cases} m_{n+1}\left(\ddot{x}_{n+1} - 2\omega\dot{z}_{n+1}\right) = F^x_{n,n+1} + F^x_A \\ m_{n+1}\left(\ddot{y}_{n+1} + \omega^2 y_{n+1}\right) = F^y_{n,n+1} + F^y_A \\ m_{n+1}\left(\ddot{z}_{n+1} + 2\omega\dot{x}_{n+1} - 3\omega^2 z_{n+1}\right) = F^z_{n,n+1} + F^z_A \end{cases} \tag{2.4}$$

where F^x_A, F^y_A and F^z_A are projection of control force from the platform in its coordinate, and m_i denotes the mass of the beads, which are expressed as:

$$m_i = \begin{cases} \dfrac{\rho l}{2} + M & i = 1 \\ \rho l & i = 2, 3, \ldots, n \\ \rho\left(\dfrac{l}{2} + \eta\right) & i = n+1 \end{cases}$$

The motion is solved by using a four-order Runge-Kutta numerical integration of Eqs. (2.3) and (2.4). In the numerical integration for deployment, new beads should be involved as shown in Fig. 2.4.

2.2 DYNAMICS MODELING AND SOLVING BASED ON RITZ METHOD

As shown in Fig. 2.5, only the tension and gravitation load are on the tether element when perturbations are ignored. Thus the acceleration of the tether element is expressed as:

$$\boldsymbol{a}(s, t) = \frac{\boldsymbol{N}(s + ds, t) - \boldsymbol{N}(s, t)}{\rho ds} \quad (\xi \le s < L) \tag{2.5}$$

where ρ denotes the density of tether, and $\boldsymbol{N}(s, t)$ denotes the tension of tether. In this section, the tension of tether is assumed to follow the Hook's Law [4], so we get:

$$\boldsymbol{N} = N\boldsymbol{\tau} = EA(|\boldsymbol{r}'| - 1)\frac{\boldsymbol{r}'}{|\boldsymbol{r}'|}$$

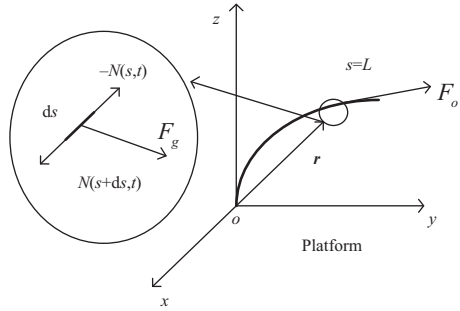

Fig. 2.5 Force analysis of each element.

where N is the magnitude of tension of the tether element, $\boldsymbol{\tau}$ is the direction vector along tangential of tether (along the direction where s increases), $\boldsymbol{r}'$ is the partial derivative of $\boldsymbol{r}$ respects to natural coordinate s, and $|\boldsymbol{r}'|$ is the module of $\boldsymbol{r}'$, written as:

$$|\boldsymbol{r}'| = \sqrt{(x')^2 + (y')^2 + (z')^2}$$

The projection of tension force is:

$$\begin{bmatrix} N_x \\ N_x \\ N_z \end{bmatrix} = EA\left(1 - \frac{1}{|\boldsymbol{r}'|}\right)\begin{bmatrix} x' \\ y' \\ z' \end{bmatrix} \tag{2.6}$$

Substituting Eq. (2.6) into Eq. (2.5), the limits of the formulas are derived as:

$$\begin{cases} \rho(\ddot{x} - 2n\dot{z}) = N_x' \\ \rho(\ddot{y} + n^2 y) = N_y' \quad (\xi \le s \le L) \\ \rho(\ddot{z} + 2n\dot{x} - 3n^2 z) = N_z' \end{cases} \tag{2.7}$$

The geometry boundary condition of the motion is:

$$x(\xi) = y(\xi) = z(\xi) = 0 \tag{2.8}$$

The stress boundary condition of the motion is:

$$\boldsymbol{N}(L) - \boldsymbol{F}_0 = \boldsymbol{0} \tag{2.9}$$

where $\boldsymbol{F}_0$ denote the terminal force from device loading on the tether. Thus, Eqs. (2.6)–(2.9) are the motion equations of the space tether. The states of the system can be solved based on the discrete equations. If the terminal

capture robot can be simplified as a mass point, the motion of it and the terminal stress can be expressed as:

$$\begin{cases} M[\ddot{x}(L) - 2\omega\dot{z}(L)] = F_{Rx} - N_x(L) \\ M[\ddot{y}(L) + \omega^2 y(L)] = F_{Ry} - N_y(L) \\ M[\ddot{z}(L) + 2\omega\dot{x}(L) - 3\omega^2 z(L)] = F_{Rz} - N_z(L) \end{cases} \tag{2.10}$$

where M is the mass of terminal robot. The simplified equations of motion of the Tethered Space Robotic System are acquired by substituting Eq. (2.7) for (2.6). The unit function $u_i(s,\xi)$, $v_i(s,\xi)$, and $w_i(s,\xi)$ are defined as:

$$\begin{cases} x(t) = \sum_{i=1}^{m} u_i(s,\xi(t))a_i(t) \\ y(t) = \sum_{i=1}^{m} v_i(s,\xi(t))b_i(t) \\ z(t) = \sum_{i=1}^{m} w_i(s,\xi(t))c_i(t) \end{cases} \tag{2.11}$$

where a_i, b_i, and c_i are the parameters in the unit functions respectively, and m is the order of the system. Since m is a limited constant, Eq. (2.11) is only the approximate solution of Eq. (2.7). To minimize the approximation error, some results are acquired by Ritz method:

$$\begin{cases} \int_{\xi}^{L} \left[\rho(\ddot{x} - 2n\dot{z}) - N_x'\right] u_i ds + \left[N_x(L) - F_{0x}\right] u_i(L) = 0 \\ \int_{\xi}^{L} \left[\rho\left(\ddot{y} + n^2 y\right) - N_y'\right] v_i ds + \left[N_y(L) - F_{0y}\right] v_i(L) = 0 \\ \int_{\xi}^{L} \left[\rho\left(\ddot{z} + 2n\dot{x} - 3n^2 z\right) - N_z'\right] w_i ds + \left[N_z(L) - F_{0z}\right] w_i(L) = 0 \end{cases}$$

To avoid the partial differential of the terms involved tension force, N_x', N_y', and N_z' are solved through integration by parts. After substituting Eq. (2.8), we have:

$$\begin{cases} \boldsymbol{M}_1\ddot{\boldsymbol{a}} + 2\dot{\xi}\boldsymbol{M}_2\dot{\boldsymbol{a}} + \left(\ddot{\xi}\boldsymbol{M}_2 + \dot{\xi}^2\boldsymbol{M}_3\right)\boldsymbol{a} - 2n\boldsymbol{M}_4\dot{\boldsymbol{c}} - 2n\dot{\xi}\boldsymbol{M}_5\boldsymbol{c} = \boldsymbol{U} \\ \boldsymbol{M}_6\ddot{\boldsymbol{b}} + 2\dot{\xi}\boldsymbol{M}_7\dot{\boldsymbol{b}} + \left(\ddot{\xi}\boldsymbol{M}_7 + \dot{\xi}^2\boldsymbol{M}_8\right)\boldsymbol{b} + n^2\boldsymbol{M}_6\boldsymbol{b} = \boldsymbol{V} \\ \boldsymbol{M}_9\ddot{\boldsymbol{c}} + 2\dot{\xi}\boldsymbol{M}_{10}\dot{\boldsymbol{c}} + \left(\ddot{\xi}\boldsymbol{M}_{10} + \dot{\xi}^2\boldsymbol{M}_{11} - 3n^2\boldsymbol{M}_9\right)\boldsymbol{c} + 2n\boldsymbol{M}_{12}\dot{\boldsymbol{a}} + 2n\dot{\xi}\boldsymbol{M}_{13}\boldsymbol{a} = \boldsymbol{W} \end{cases} \tag{2.12}$$

where $\boldsymbol{a}$, $\boldsymbol{b}$, and $\boldsymbol{c}$ are coefficient vectors, where $\boldsymbol{a} = (a_1, \ldots, a_m)^T$, $\boldsymbol{b} = (b_1, \ldots, b_m)^T$, and $\boldsymbol{c} = (c_1, \ldots, c_m)^T$. $\boldsymbol{M}_k$ is defined as:

$$\boldsymbol{M}_1 = \left[\int_\xi^L u_i u_j ds\right], \boldsymbol{M}_2 = \left[\int_\xi^L u_i \frac{\partial u_j}{\partial \xi} ds\right], \boldsymbol{M}_3 = \left[\int_\xi^L u_i \frac{\partial^2 u_j}{\partial \xi^2} ds\right],$$
$$\boldsymbol{M}_4 = \left[\int_\xi^L u_i w_j ds\right], \boldsymbol{M}_5 = \left[\int_\xi^L u_i \frac{\partial w_j}{\partial \xi} ds\right], \boldsymbol{M}_6 = \left[\int_\xi^L v_i v_j ds\right],$$
$$\boldsymbol{M}_7 = \left[\int_\xi^L v_i \frac{\partial v_j}{\partial \xi} ds\right], \boldsymbol{M}_8 = \left[\int_\xi^L v_i \frac{\partial^2 v_j}{\partial \xi^2} ds\right], \boldsymbol{M}_9 = \left[\int_\xi^L w_i w_j ds\right],$$
$$\boldsymbol{M}_{10} = \left[\int_\xi^L w_i \frac{\partial w_j}{\partial \xi} ds\right], \boldsymbol{M}_{11} = \left[\int_\xi^L w_i \frac{\partial^2 w_j}{\partial \xi^2} ds\right],$$
$$\boldsymbol{M}_{12} = \left[\int_\xi^L w_i u_j ds\right], \boldsymbol{M}_{13} = \left[\int_\xi^L w_i \frac{\partial u_j}{\partial \xi} ds\right]$$

where $i = 1, \ldots, m$, $j = 1, \ldots, m$; $\boldsymbol{U}$, $\boldsymbol{V}$, and $\boldsymbol{W}$ are defined as:

$$\boldsymbol{U} = -F_{0x}\boldsymbol{u}(L) - \int_\xi^L N_x \frac{\partial \boldsymbol{u}}{\partial s} ds$$
$$\boldsymbol{V} = -F_{0y}\boldsymbol{v}(L) - \int_\xi^L N_y \frac{\partial \boldsymbol{v}}{\partial s} ds$$
$$\boldsymbol{W} = -F_{0z}\boldsymbol{w}(L) - \int_\xi^L N_z \frac{\partial \boldsymbol{w}}{\partial s} ds$$

where $\boldsymbol{u}$, $\boldsymbol{v}$, $\boldsymbol{w}$ are column vector defined by unite functions, namely $\boldsymbol{u} = (u_1, \ldots, u_m)^T$, $\boldsymbol{v} = (v_1, \ldots, v_m)^T$, and $\boldsymbol{w} = (w_1, \ldots, w_m)^T$.

The system of ordinary differential equations (2.12) includes $3m$ ordinary differential equations regarding to time. Numerical integration can be used for solving parameters in $3m$ ordinary differential equations, based on the terminal force $\boldsymbol{F}_0$ and acceleration $\ddot{\xi}$. According to the reference, the system order is set to be $m = 3$ and the unit functions are:

$$u_i = v_i = w_i = (s - \xi)^i \quad (i = 1, 2, 3)$$

In addition, the motion of TSRS can be acquired based on the simplified equations after the same derivation by substitute equation (2.10) for (2.9).

2.3 DYNAMICS MODELING AND SOLVING BASED ON HYBRID UNIT METHOD

Both the Ritz method and Bead model are the classic methods to solve the dynamics of space tether. However, both these two method have disadvantages. As the length increases, the accuracy of the Ritz method decreases sharply, according to the sharp augment of ill-conditioning of the equivalent mass matrixes $\boldsymbol{M}_1$, $\boldsymbol{M}_6$, and $\boldsymbol{M}_9$ in Eq. (2.11). The Bead model is defined by treating the factor of different tension between two adjacent elastic link and the bead mass as the acceleration of the bead. This definition leads to serious ill-conditioning and unreliable calculation of Eqs. (2.3) and (2.4). In addition, the assumption of the elastic link in the Bead model is too simple, which may result in divergence when the tension of the tether changes suddenly and rapidly.

During the deployment of the TSRS, the deployed velocity of the tether is the main control variable. So the tension around the proximity of the deployment point changes severely. In this case, the Ritz method and Bead model should be combined to solve this issue. As shown in Fig. 2.6, the Ritz method is used to solve the tether around the proximity of the deployment point, while the Bead model is used to calculate the tether segments. This method restricts the length of the tether segment based on the Ritz method,

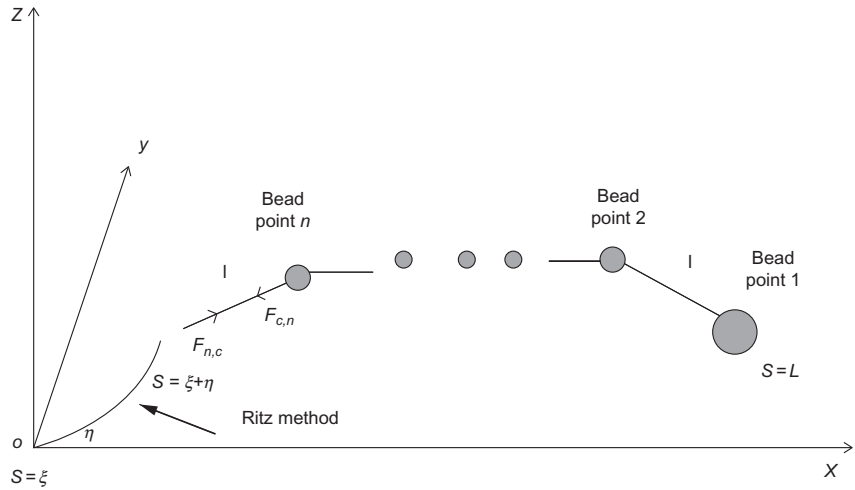

Fig. 2.6 Hybrid unit method.

which ensures the accuracy and efficiency of the Ritz method. On the other hand, an anchor point should be involved to enhance accuracy and efficiency.

For the tether segment between the deployment point O and the hybrid point C, the motion is still under Eq. (2.7) and the geometry boundary condition (2.8), but the domain of equation changes from $[\xi,\ L]$ to $[\xi, \xi+\eta]$. The stress boundary condition is:

$$\boldsymbol{N}(\xi+\eta)-\boldsymbol{F}_{n,c}=\boldsymbol{0}$$

The same derivation is used as mentioned in Section 2.2, then we get:

$$\begin{cases} \boldsymbol{M}_1\ddot{\boldsymbol{a}}+2\dot{\xi}\boldsymbol{M}_2\dot{\boldsymbol{a}}+\left(\ddot{\xi}\boldsymbol{M}_2+\dot{\xi}^2\boldsymbol{M}_3\right)\boldsymbol{a}-2n\boldsymbol{M}_4\dot{\boldsymbol{c}}-2n\dot{\xi}\boldsymbol{M}_5\boldsymbol{c}=\boldsymbol{U}_i \\ \boldsymbol{M}_6\ddot{\boldsymbol{b}}+2\dot{\xi}\boldsymbol{M}_7\dot{\boldsymbol{b}}+\left(\ddot{\xi}\boldsymbol{M}_7+\dot{\xi}^2\boldsymbol{M}_8\right)\boldsymbol{b}+n^2\boldsymbol{M}_6\boldsymbol{b}=\boldsymbol{V}_i \\ \boldsymbol{M}_9\ddot{\boldsymbol{c}}+2\dot{\xi}\boldsymbol{M}_{10}\dot{\boldsymbol{c}}+\left(\ddot{\xi}\boldsymbol{M}_{10}+\dot{\xi}^2\boldsymbol{M}_{11}-3n^2\boldsymbol{M}_9\right)\boldsymbol{c}+2n\boldsymbol{M}_{12}\dot{\boldsymbol{a}}+2n\dot{\xi}\boldsymbol{M}_{13}\boldsymbol{a}=\boldsymbol{W}_i \end{cases} \tag{2.13}$$

where the calculation of matrix $\boldsymbol{M}_k(k=1,\ldots,13)$ and vectors $\boldsymbol{U}$, $\boldsymbol{V}$, $\boldsymbol{W}$ are the same with them in Eq. (2.12), and the only difference is the integrating range changed to be $[\xi, \xi+\eta]$.

For the tether segment from point C to the terminal device, a simple bead model is used to discrete the system. As mentioned in Section 2.1, the motion equations of the beads are derived as:

$$\begin{cases} \ddot{x}_i-2\omega\dot{z}_i=\dfrac{1}{m_i}\left(F^x_{i-1,i}+F^x_{i+1,i}\right) \\ \ddot{y}_i+\omega^2 y_i=\dfrac{1}{m_i}\left(F^y_{i-1,i}+F^y_{i+1,i}\right) \quad (i=1,2,\ldots,n) \\ \ddot{z}_i+2\omega\dot{x}_i-3\omega^2 z_i=\dfrac{1}{m_i}\left(F^z_{i-1,i}+F^z_{i+1,i}\right) \end{cases} \tag{2.14}$$

where $F^x_{n+1,n}=F^x_{c,n}$, $F^y_{n+1,n}=F^y_{c,n}$, $F^z_{n+1,n}=F^z_{c,n}$.

To solve the ordinary differential equations (2.13) and (2.14), elastic force $\boldsymbol{F}_{c,n}$ and $\boldsymbol{F}_{n,c}$, and the deployment acceleration of tether $\ddot{\xi}$ are necessary. From the Hook's Law, we can get:

$$\boldsymbol{F}_{c,n}=-\boldsymbol{F}_{n,c}=EA\left(\frac{|\boldsymbol{r}_{c,n}|}{l}-1\right)\frac{\boldsymbol{r}_{c,n}}{|\boldsymbol{r}_{c,n}|} \tag{2.15}$$

where

$$\boldsymbol{r}_{c,n} = \begin{bmatrix} x_n - \sum_{i=1}^{m} a_i u_i(\xi + \eta) \\ y_n - \sum_{i=1}^{m} b_i v_i(\xi + \eta) \\ z_n - \sum_{i=1}^{m} c_i w_i(\xi + \eta) \end{bmatrix}$$

The deployment acceleration of the tether $\ddot{\xi}$ is defined by the deployment controller, which can be expressed as:

$$\ddot{\xi} = f(r, \dot{r}, \ddot{r}) \tag{2.16}$$

The hybrid method are composed by Eqs. (2.13)–(2.16). The numerical integration method can be used for solving these ordinary differential equations, while Eq. (2.13) will be useless as η is growing. To limit η, a scheme of bead increase should be introduced.

If the natural length of tether η between the deployment point and C point is larger than $\eta_{\max}$, namely $\eta > \eta_{\max}$, a new natural length of tether l is segmented from this segment, as shown in Fig. 2.7. Thus a new hybrid point generates, and the old hybrid point turns to be a normal bead. The new hybrid point is:

$$\begin{cases} x_c = \sum_{i=1}^{m} u_i(\eta - l) a_i \\ y_c = \sum_{i=1}^{m} v_i(\eta - l) b_i \\ z_c = \sum_{i=1}^{m} w_i(\eta - l) c_i \end{cases}$$

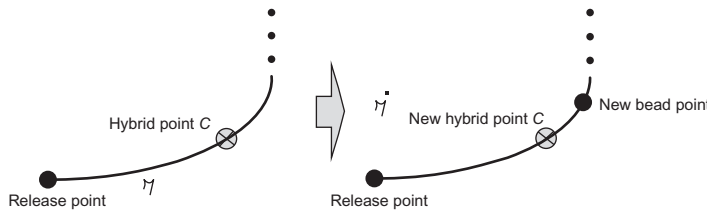

Fig. 2.7 Increase of beads.

This scheme of bead increase limits the length of each tether segment to be no longer than $\eta_{\max}$, which ensures the effectiveness of the Ritz method.

2.4 DYNAMICS MODELING AND SOLVING BASED ON NEWTON-EULER METHOD

We have discussed the Bead model and the Ritz method based on Hook's Law. In this section, Newton-Euler method is introduced to derive the dynamics model of the system when the characteristic of the release mechanics are taken into account, and the tether does not fulfill Hook's Law because the characteristic that only tension, but not stress, is reasonable on the tether. There are some assumptions for the Space Tethered Robot System shown in the Fig. 2.1:

(1) The TSRS consists of a platform satellite B, a terminal capture device A, and connection tether, where the platform and capture device are assumed to be mass points, as shown in Figs. 2.8 and 2.9.

(2) When the mass of platform satellite B is much heavier than the terminal capture device A and the flexible tether, the center of mass of the whole system is assumed to be at the center of mass of platform B, and the center of mass is assumed to be coincidence with the center of motion.

(3) A circular Keplerian reference orbit is assumed for the motion of center of mass of the system.

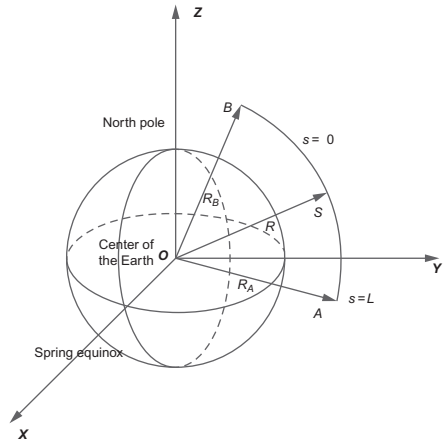

Fig. 2.8 Earth inertial coordinate system.

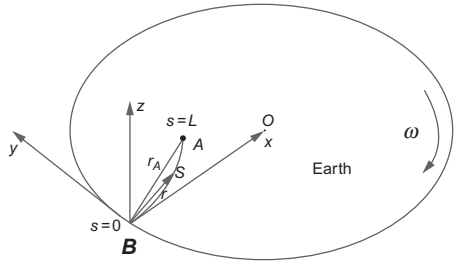

Fig. 2.9 Orbit coordinate system.

(4) The tether is assumed to be an ideal tether, so neither compression resistance nor bend resistance is available on this tether.

(5) The tether is uniform in mass, and the characteristics of each element are the same.

An Earth-equatorial coordinate *OXYZ* is defined to describe the motion of system. This coordinate has the origin at the center of Earth, *X*-axis along the intersecting lines of equatorial plane and ecliptic plane towards Vernal Equinoctial Point, *Z*-axis towards North Pole, *Y*-axis completing the right hand triad, as shown in Fig. 2.8. Orbit coordinate system is defined as *Bxyz*, where the origin is at the center of mass of the platform satellite B, *x*-axis points to center of the Earth, *y*-axis is opposite to velocity direction of platform B, *z*-axis completing the right hand triad, as shown in Fig. 2.9.

A flexible tether is shown in Fig. 2.10. Similar to the definition in Section 2.1, a variable *s* is introduced to describe the length of tether *BC*

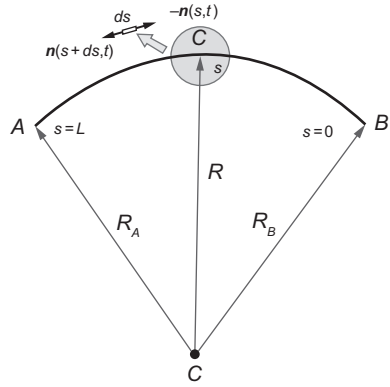

Fig. 2.10 Natural coordinate of tether.

before deformation, namely the natural length of BC. So for point B, s_B is zero, while for point A, s_A is L, where L is the natural length.

According to the material mechanics, strain on point C fulfills the equation as:

$$\varepsilon = \left|\frac{\partial \boldsymbol{R}}{\partial s}\right| - 1 \tag{2.17}$$

The tangent vector on point C fulfills the equation as:

$$\boldsymbol{\tau} = \frac{\partial \boldsymbol{R} / \partial s}{\left|\partial \boldsymbol{R} / \partial s\right|} \tag{2.18}$$

On the strength of Kelvin-Voigt Law, and the characteristic that only tension resistance but not compression resistance can be loaded on the tether, the tension of point C is expressed as:

$$\boldsymbol{n}(s,t) = \begin{cases} EA(\varepsilon + \alpha\dot{\varepsilon})\boldsymbol{\tau} & \varepsilon \geq 0 \\ 0 & \varepsilon < 0 \end{cases} \tag{2.19}$$

where E denotes the Young's Module of tether, A denotes the cross-sectional area of tether, α denotes the viscous damping coefficient of tether.

A force analysis of infinitesimal element ds in Fig. 2.10 is shown in Fig. 2.11. We have:

$$\rho ds \frac{\partial^2}{\partial t^2}\boldsymbol{R}(s,t) = \boldsymbol{n}(s+ds,t) - \boldsymbol{n}(s,t) - \mu_e \frac{\boldsymbol{R}}{R^3}\rho ds + \boldsymbol{f}\,ds$$

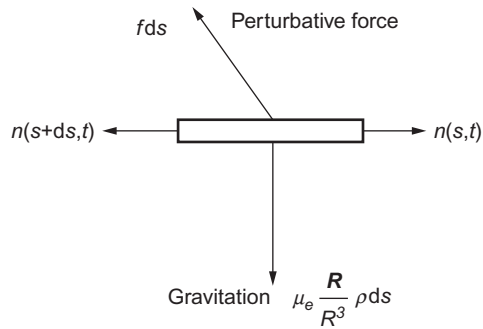

Fig. 2.11 Force analysis of a infinitesimal segment.

where ρ denotes density of the tether, μ_e is the gravitational constant of the Earth, $\boldsymbol{f}$ is the distribution density of perturbation force loading on the tether. In the previous equation, when $ds \to 0$, we can get:

$$\frac{\partial^2}{\partial t^2}\boldsymbol{R}(s,t) = \frac{1}{\rho}\frac{\partial \boldsymbol{n}(s,t)}{\partial s} - \mu_e \frac{\boldsymbol{R}}{R^3} + \boldsymbol{f} \tag{2.20}$$

The orbit of platform B is known, thus we get:

$$\boldsymbol{R}(0,t) = \boldsymbol{R}_B(t) \tag{2.21}$$

The force analysis of terminal device A is shown in Fig. 2.12, whose motion fulfills the equation as:

$$m_A \frac{\partial^2 \boldsymbol{R}(L,t)}{\partial t^2} = -\boldsymbol{n}(L,t) - m_A \mu_e \frac{\boldsymbol{R}(L,t)}{R^3} + \boldsymbol{F} \tag{2.22}$$

where m_A the mass of terminal capture device, $\boldsymbol{F}$ the perturbation force loading on the device A.

Eqs. (2.17)–(2.22) are the motion of dynamics with respect to the inertia

Earth coordinate. However, the solving of motion equations is very complicated due to $|\boldsymbol{R}| \gg L$. So we change the motion equations with respect to the inertia

Earth coordinate to the orbit coordinate, as shown in Figs. 2.11 and 2.12. Because:

$$\boldsymbol{R} = \boldsymbol{R}_B + \boldsymbol{r}$$

Thus:

$$\frac{\partial^2 \boldsymbol{R}}{\partial t^2} = \frac{d^2 \boldsymbol{R}_B}{dt^2} + \frac{\partial^2 \boldsymbol{r}}{\partial t^2} \tag{2.23}$$

In the orbit coordinate system, $\boldsymbol{r}$ fulfills the equations as:

$$\boldsymbol{r} = (x, y, z)^T = x\boldsymbol{i} + y\boldsymbol{j} + z\boldsymbol{k}$$

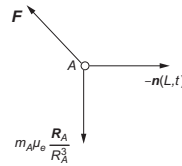

Fig. 2.12 Force analysis of terminal capture device.

where $\boldsymbol{i}, \boldsymbol{j}, \boldsymbol{k}$ represent the unit vectors of three axis of orbit coordinate system. In addition, we define:

$$\dot{\boldsymbol{r}} = \left(\frac{\partial x}{\partial t}, \frac{\partial y}{\partial t}, \frac{\partial z}{\partial t}\right)^T = \frac{\partial x}{\partial t}\boldsymbol{i} + \frac{\partial y}{\partial t}\boldsymbol{j} + \frac{\partial z}{\partial t}\boldsymbol{k}$$

we get:

$$\frac{\partial \boldsymbol{r}}{\partial t} = \frac{\partial x}{\partial t}\boldsymbol{i} + \frac{\partial y}{\partial t}\boldsymbol{j} + \frac{\partial z}{\partial t}\boldsymbol{k} + x\frac{\partial \boldsymbol{i}}{\partial t} + y\frac{\partial \boldsymbol{j}}{\partial t} + z\frac{\partial \boldsymbol{k}}{\partial t}$$

Substituting the Poisson formula into the previous equation, we get:

$$\frac{\partial \boldsymbol{r}}{\partial t} = \dot{\boldsymbol{r}} + \omega \times \boldsymbol{r} \tag{2.24}$$

After time differential of the previous equation, we get:

$$\frac{\partial^2 \boldsymbol{r}}{\partial t^2} = \ddot{\boldsymbol{r}} + \dot{\omega} \times \boldsymbol{r} + 2\omega \times \dot{\boldsymbol{r}} + \omega \times (\omega \times \boldsymbol{r}) \tag{2.25}$$

In addition, we assume that the platform B motions on a Keplerian orbit, we get:

$$\frac{d^2 \boldsymbol{R}_B}{dt^2} = -\mu_e \frac{\boldsymbol{R}_B}{R_B^3}$$

Thus we get:

$$\frac{\partial^2 \boldsymbol{R}}{\partial t^2} = \ddot{\boldsymbol{r}} + \dot{\omega} \times \boldsymbol{r} + 2\omega \times \dot{\boldsymbol{r}} + \omega \times (\omega \times \boldsymbol{r}) - \mu_e \frac{\boldsymbol{R}_B}{R_B^3} \tag{2.26}$$

Substituting the previous equation into (2.20), we get:

$$\ddot{\boldsymbol{r}} + \dot{\omega} \times \boldsymbol{r} + 2\omega \times \dot{\boldsymbol{r}} + \omega \times (\omega \times \boldsymbol{r}) + \mu_e \left(\frac{\boldsymbol{R}}{R^3} - \frac{\boldsymbol{R}_B}{R_B^3}\right) = \frac{1}{\rho}\frac{\partial \boldsymbol{n}}{\partial s} + \frac{\boldsymbol{f}}{\rho}$$

The first order approximation of $\boldsymbol{R}/R^3$ around $\boldsymbol{R}_B$ is:

$$\frac{\boldsymbol{R}}{R^3} - \frac{\boldsymbol{R}_B}{R_B^3} \approx \frac{\boldsymbol{r}}{R_B^3} - 3(\boldsymbol{r} \cdot \boldsymbol{R}_B)\frac{\boldsymbol{R}_B}{R_B^5}$$

So the motion equations of flexible tether with respect to orbit coordinate is:

$$\ddot{\boldsymbol{r}} + \dot{\omega} \times \boldsymbol{r} + 2\omega \times \dot{\boldsymbol{r}} + \omega \times (\omega \times \boldsymbol{r}) + \mu_e \left[\frac{\boldsymbol{r}}{R_B^3} - 3(\boldsymbol{r} \cdot \boldsymbol{R}_B)\frac{\boldsymbol{R}_B}{R_B^5}\right] = \frac{1}{\rho}\frac{\partial \boldsymbol{n}}{\partial s} + \frac{\boldsymbol{f}}{\rho}$$

Define $\boldsymbol{p}$ as:

$$\boldsymbol{p}(s,t)\triangleq\dot{\boldsymbol{\omega}}\times\boldsymbol{r}+2\boldsymbol{\omega}\times\dot{\boldsymbol{r}}+\boldsymbol{\omega}\times(\boldsymbol{\omega}\times\boldsymbol{r})+\mu_e\left[\frac{\boldsymbol{r}}{R_B^3}-3(\boldsymbol{r}\cdot\boldsymbol{R}_B)\frac{\boldsymbol{R}_B}{R_B^5}\right]$$

So the dynamics equation of tether can be expressed as:

$$\ddot{\boldsymbol{r}}+\boldsymbol{p}=\frac{1}{\rho}\frac{\partial\boldsymbol{n}}{\partial s}+\frac{\boldsymbol{f}}{\rho}\quad s\in[0,L] \tag{2.27}$$

In addition, boundary condition (2.21) can be transformed as:

$$\boldsymbol{r}(0,t)=\boldsymbol{0} \tag{2.28}$$

Boundary condition (2.22) can be transformed as:

$$m_A[\ddot{\boldsymbol{r}}(L,t)+\boldsymbol{p}(L,t)]=-\boldsymbol{n}(L,t)+\boldsymbol{F} \tag{2.29}$$

Eqs. (2.17)–(2.19), (2.27)–(2.29) constitute the mathematical model of the TSRS in station-keeping phase:

$$\begin{cases}\ddot{\boldsymbol{r}}+\boldsymbol{p}=\dfrac{1}{\rho}\dfrac{\partial\boldsymbol{n}}{\partial s}+\dfrac{\boldsymbol{f}}{\rho}\quad s\in(0,L)\\ \boldsymbol{r}(0,t)=0, m_A[\ddot{\boldsymbol{r}}(L,t)+\boldsymbol{p}(L,t)]=-\boldsymbol{n}(L,t)+\boldsymbol{F}\\ \varepsilon=\left|\dfrac{\partial\boldsymbol{r}}{\partial s}\right|-1, \boldsymbol{\tau}=\dfrac{\partial\boldsymbol{r}/\partial s}{\left|\partial\boldsymbol{r}/\partial s\right|}\\ \boldsymbol{n}(s,t)=\begin{cases}EA(\varepsilon+\alpha\dot{\varepsilon})\boldsymbol{\tau} & \varepsilon\geq 0\\ 0 & \varepsilon<0\end{cases}\end{cases} \tag{2.30}$$

This is a set of partial differential equations, which are not classic ellipse, parabola, or hyperbola partial differential equations. Thus it is a highly challenging to solve these equations. We will discuss the method to solve this issue.

Based on the assumptions of the TSRS, we will analyze the deployment and retrieval in detail. For analysis, we make some assumptions to simplify the deployment/retrieval mechanism: (1) The mechanism of deployment and retrieval is a capstan which is uniform in mass, and the center of mass coincides to the geometry center, as shown in Fig. 2.13. (2) The center of the capstan coincides to the center of mass of platform B, and the revolution axis of the capstan coincides to the z-axis of orbit coordinate. (3) On the tether segment CD, tension of tether is constant, and the natural length of tether segment DE is approximate constant. (4) The tension

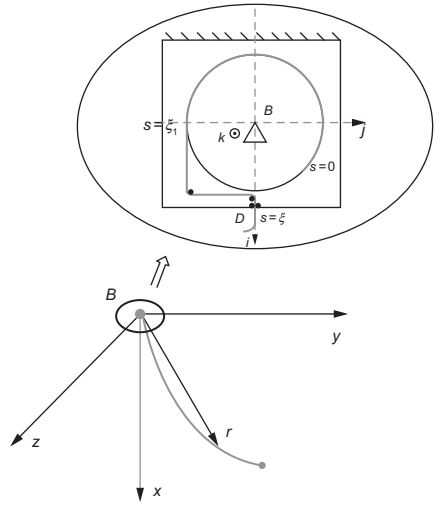

Fig. 2.13 Schematic of the deployment and retrieval mechanisms.

of flexible tether on the capstan is constant zero, and there is no strain force towards the revolution axis loading on the tether. (5) The thickness of the winding tether can be ignored, and the center of mass of the capstan is assumed always on the geometry center.

Although the length varies constantly, the force of each element of the tether is the same with example shown in Fig. 2.13. So the equation of motion of the tether is:

$$\ddot{\boldsymbol{r}} + \boldsymbol{p} = \frac{1}{\rho}\frac{\partial \boldsymbol{n}}{\partial s} + \frac{\boldsymbol{f}}{\rho} \quad s \in [\xi, L] \tag{2.31}$$

The boundary condition equation (2.28) can be rewritten as:

$$\boldsymbol{r}(\xi, t) = \boldsymbol{r}_D \tag{2.32}$$

The force analysis of terminal device A is the same with Fig. 2.13. So the boundary condition equation (2.29) does not change, which is still in the expression:

$$m_A[\ddot{\boldsymbol{r}}(L, t) + \boldsymbol{p}(L, t)] = -\boldsymbol{n}(L, t) + \boldsymbol{F} \tag{2.33}$$

Because a new variable ξ is introduced in Eq. (2.31), supplementary equations are needed to accomplish the dynamics model.

The schematic of the capstan is shown in Fig. 2.14. If it works in the deployment phase, the total momentum of the capstan and tether at t moment is shown as:

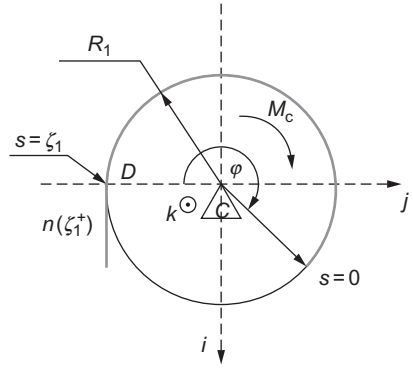

Fig. 2.14 Schematic of capstan (***i***, ***j***, and ***k*** are corresponding to the axis of orbit coordinate system).

$$\boldsymbol{H}(t)=\left[I_1+\rho R_1^3\varphi(t)\right][\dot{\varphi}(t)+\omega(t)]\boldsymbol{k}$$

where I_1 is the moment of inertia of the capstan, R_1 is the radius of the capstan, and ω is the angular velocity. At the $t+dt$ moment, because tether in $|d\xi_1|$ length departs from the capstan, the total momentum with respect to the revolution axis of the capstan changes to be:

$$\boldsymbol{H}(t+dt)=\left[I_1+\rho R_1^3\varphi(t+dt)\right][\dot{\varphi}(t+dt)+\omega(t+dt)]\boldsymbol{k}+\rho|d\xi_1|R_1\boldsymbol{j}\times\left.\frac{\partial\boldsymbol{R}}{\partial t}\right|_{s=\xi_1^+}$$

where

$d\xi_1<0$ (as tether releasing, ξ_1 decreases constantly)

$$\begin{aligned}\left.\frac{\partial\boldsymbol{R}}{\partial t}\right|_{s=\xi_1^+}&=\left.\frac{\partial}{\partial t}[-R_B\boldsymbol{i}+\boldsymbol{r}(s,t)]\right|_{s=\xi_1^+}\\&=-R_B\omega\boldsymbol{j}+\left.\frac{\partial}{\partial t}\boldsymbol{r}(s,t)\right|_{s=\xi_1^+}\\&=-R_B\omega\boldsymbol{j}+\left.\frac{d}{dt}\boldsymbol{r}(s,t)\right|_{s=\xi_1^+}-\left.\frac{\partial}{\partial s}\boldsymbol{r}(s,t)\right|_{s=\xi_1^+(t)}\frac{d\xi_1}{dt}\\&=-R_B\omega\boldsymbol{j}-R_1\omega\boldsymbol{i}-\left(\varepsilon_{\xi_1^+}+1\right)\frac{d\xi_1}{dt}\boldsymbol{i}\end{aligned}$$

then

$$\boldsymbol{j}\times\frac{\partial \boldsymbol{R}}{\partial t}\bigg|_{s=\xi_1^+}=R_1\omega\boldsymbol{k}+\left(\varepsilon_{\xi_1^+}+1\right)\frac{d\xi_1}{dt}\boldsymbol{k}$$

From the moment of momentum theorem, we have:

$$\lim_{t\to 0}\frac{\boldsymbol{H}(t+dt)-\boldsymbol{H}(t)}{dt}=M_C\boldsymbol{k}+R_1\boldsymbol{j}\times\boldsymbol{n}\left(\xi_1^+\right)$$

Another equation can be get from the assumption:

$$\xi_1=R_1\varphi$$

The derivation can be acquired from the above-mentioned equations:

$$\left(I_1+\rho\varphi R_1^3\right)\ddot{\varphi}-\rho R_1^3\varepsilon|_{\xi_1^+}\dot{\varphi}^2+\left(I_1+\rho\varphi R_1^3\right)\dot{\omega}=M_C-R_1\left|\boldsymbol{n}\left(\xi_1^+\right)\right| \quad (2.34)$$

According to the relationship between point C and point D in the assumption, we get:

$$\xi-\xi_1=const\quad \varepsilon|_{\xi_1^+}=\varepsilon|_{\xi}\quad \left|\boldsymbol{n}\left(\xi_1^+\right)\right|=|\boldsymbol{n}(\xi)| \quad (2.35)$$

If it works at t moment in the retrieval phase, the total momentum of the capstan, tether winding on the capstan, and the tether segment in length $|d\xi_1|$ that will be twisted on the capstan in $t+dt$ moment is expressed as:

$$\boldsymbol{H}(t)=\left[I_1+\rho R_1^3\varphi(t)\right][\dot{\varphi}(t)+\omega(t)]\boldsymbol{k}+\rho|d\xi_1|R_1\boldsymbol{j}\times\frac{\partial \boldsymbol{R}}{\partial t}\bigg|_{s=\xi_1^+}$$

In which, $d\xi_1>0$. At $t+dt$ moment, the tether segment in length $|d\xi_1|$ twisted on the capstan, so the total momentum with respect to the rotation axis of the capstan is changed to be:

$$\boldsymbol{H}(t+dt)=\left[I_1+\rho R_1^3\varphi(t+dt)\right][\dot{\varphi}(t+dt)+\omega(t+dt)]\boldsymbol{k}$$

Similarly as the derivation in the deployment phase, we get:

$$\left(I_1+\rho\varphi R_1^3\right)\ddot{\varphi}-\rho R_1^3\varepsilon|_{\xi_1^+}\dot{\varphi}^2+\left(I_1+\rho\varphi R_1^3\right)\dot{\omega}=M_C-R_1\left|\boldsymbol{n}\left(\xi_1^+\right)\right| \quad (2.36)$$

The equations described the motion of the capstan (2.34) and (2.36) are consistent, which indicates that the formulas of capstan motion during deployment and retrieval are the same. So Eqs. (2.17)–(2.19), (2.31)–(2.34), and (2.36) consist of the system of equations for deployment and retrieval:

$$\begin{cases} \ddot{\boldsymbol{r}} + \boldsymbol{p} = \dfrac{1}{\rho}\dfrac{\partial \boldsymbol{n}}{\partial s} + \dfrac{\boldsymbol{f}}{\rho} \quad s \in (\xi, L) \\ \boldsymbol{r}(\xi, t) = \boldsymbol{r}_D, m_A[\ddot{\boldsymbol{r}}(L,t) + \boldsymbol{p}(L,t)] = -\boldsymbol{n}(L,t) + \boldsymbol{F} \\ \left(I_1 + \rho\varphi R_1^3\right)\ddot{\varphi} - \rho R_1^3 \varepsilon|_{\xi_1^+}\dot{\varphi}^2 + \left(I_1 + \rho\varphi R_1^3\right)\dot{\omega} = M_C - R_1\left|\boldsymbol{n}\left(\xi_1^+\right)\right| \\ \xi - \xi_1 = const \quad \varepsilon|_{\xi_1^+} = \varepsilon|_{\xi} \quad \left|\boldsymbol{n}\left(\xi_1^+\right)\right| = |\boldsymbol{n}(\xi)| \\ \varepsilon = \left|\dfrac{\partial \boldsymbol{r}}{\partial s}\right| - 1, \boldsymbol{\tau} = \dfrac{{}^{\partial r}/_{\partial s}}{\left|{}^{\partial r}/_{\partial s}\right|} \\ \boldsymbol{n}(s,t) = \begin{cases} EA(\varepsilon + \alpha\dot{\varepsilon})\boldsymbol{\tau} & \varepsilon \geq 0 \\ 0 & \varepsilon < 0 \end{cases} \end{cases} \tag{2.37}$$

It is a set of nonlinear partial differential equations. Compared to Eq. (2.30), the solving is more difficult, because the definition domain varies with time. So the solving of equations is very important.

The motion of the tether can be disintegrated into three parts as shown in the Fig. 2.15. (1) The velocity of tether swing motion as shown in Fig. 2.15A is very slow. (2) The velocity of tether lateral oscillation shown in Fig. 2.15B

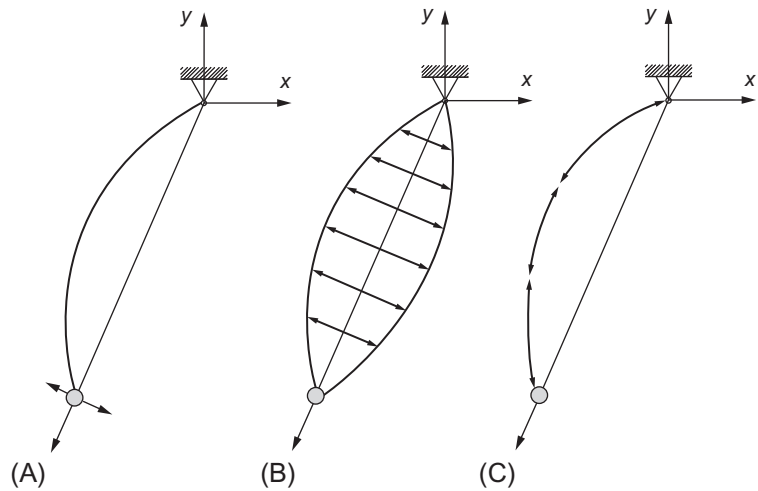

Fig. 2.15 Motion analysis of the tether. (A) The velocity of tether lateral oscillation; (B) the velocities of lateral oscillations of tether's nodes; (C) the velocity of tether longitudinal oscillation.

is also very slow. (3) The velocity of tether longitudinal oscillation shown in Fig. 2.15C is very quick. Because the dynamics model of the system composes motions in different time scale, the dynamics model of the system is ill-conditioned.

The ill-conditioned characteristic of the space tethered system does not affect the correctness of the dynamics model. But the computation efficiency will sharply decline, if this ill-conditioned characteristic is not taken into account. To solve this problem, some things should be remarked in the calculation. (1) Time integrators should be selected carefully. (2) Variables should be selected carefully. For remark (1), some special integration methods could be considered, as Gill method. For remark (2), we need to separate the quick changed variables from slow changed variables. With regard to the simplified dynamics model of the TSRS, we do not use conventional Cartesian coordinates to describe the motion, but use a similar method mentioned in the reference, in which the axial strain ε and the unit tangential vector $\boldsymbol{\tau}$ are used to describe the motion and transform of the tether. In this case, the axial quick changed variable and lateral slow changed variable are separated from each other. Based on this, we calculate the strain in small step, and lateral motion in bigger step. So the calculating speed is enhanced.

According to Eq. (2.17), (2.18), and (2.28), we get:

$$\boldsymbol{r}(s,t)=\int_0^s(1+\varepsilon)\boldsymbol{\tau}d\sigma$$

where both σ and s are the natural coordinate of the tether, so we introduce σ to distinguish them. A new variable $\boldsymbol{q}(s,t)$ is introduced and defined as:

$$\boldsymbol{q}(s,t)\underline{\underline{\Delta}}\dot{\boldsymbol{\omega}}\times[(1+\varepsilon)\boldsymbol{\tau}]+2\boldsymbol{\omega}\times[(1+\varepsilon)\boldsymbol{\tau}]^{\cdot}+\boldsymbol{\omega}\times\{\boldsymbol{\omega}\times[(1+\varepsilon)\boldsymbol{\tau}]\}$$
$$+\mu_e\left\{\frac{(1+\varepsilon)\boldsymbol{\tau}}{R_B^3}-3\{[(1+\varepsilon)\boldsymbol{\tau}]\cdot\boldsymbol{R}_B\}\frac{\boldsymbol{R}_B}{R_B^5}\right\}$$

According to the definition of $\boldsymbol{p}(s,t)$, we get:

$$\boldsymbol{p}(s,t)=\int_0^s\boldsymbol{q}(s,t)d\sigma$$

Integrate the left terms of Eq. (2.11) with respect to σ:

$$\int_s^L (\ddot{\boldsymbol{r}}+\boldsymbol{p})d\sigma = (\ddot{\boldsymbol{r}}+\boldsymbol{p})\sigma|_s^L - \int_s^L (\ddot{\boldsymbol{r}}'+\boldsymbol{p}')\sigma d\sigma$$

$$= [\ddot{\boldsymbol{r}}(L)+\boldsymbol{p}(L)]L - [\ddot{\boldsymbol{r}}(s)+\boldsymbol{p}(s)]s - \int_s^L \{[(1+\varepsilon)\boldsymbol{\tau}]^{\cdot\cdot} + \boldsymbol{q}\}\sigma d\sigma$$

$$= \int_0^L \{[(1+\varepsilon)\boldsymbol{\tau}]^{\cdot\cdot} + \boldsymbol{q}\}Ld\sigma - \int_0^s \{[(1+\varepsilon)\boldsymbol{\tau}]^{\cdot\cdot} + \boldsymbol{q}\}sd\sigma$$

$$- \int_s^L \{[(1+\varepsilon)\boldsymbol{\tau}]^{\cdot\cdot} + \boldsymbol{q}\}\sigma d\sigma = \int_0^L G\{[(1+\varepsilon)\boldsymbol{\tau}]^{\cdot\cdot} + \boldsymbol{q}\}d\sigma$$

where $(\,)'$ denotes partial differential with respect to variable s, $G = L - \max(s, \sigma)$. Integrate Eq. (2.11) with respect to σ:

$$\int_0^L G\{[(1+\varepsilon)\boldsymbol{\tau}]^{\cdot\cdot} + \boldsymbol{q}\}d\sigma = \frac{1}{\rho}[\boldsymbol{n}(L) - \boldsymbol{n}(s)] + \int_s^L \frac{\boldsymbol{f}}{\rho}d\sigma$$

From Eq. (2.13), we have:

$$\boldsymbol{n}(L,t) = \boldsymbol{F} - m_A[\ddot{\boldsymbol{r}}(L) + \boldsymbol{p}(L)]$$

Substitute the above integration equation, we get:

$$\int_0^L \hat{G}\{[(1+\varepsilon)\boldsymbol{\tau}]^{\cdot\cdot} + \boldsymbol{q}\}d\sigma = \frac{\boldsymbol{F}}{\rho} + \int_s^L \frac{\boldsymbol{f}}{\rho}d\sigma - \frac{\boldsymbol{n}(s)}{\rho} \tag{2.38}$$

where $\hat{G} = \frac{m_A}{\rho} + L - \max(s, \sigma)$.

Eq. (2.38) is the integration of the TSRS during the station-keeping phase. The partial differential terms with respect to natural coordinate s is removed via integration. Besides, the new integration equation includes both motion equation and boundary condition, which easies the discrete in next step. Then, linear interpolation is used for discretization.

For the integration:

$$I = \int_a^b f(x)dx$$

In this section, $[a, b]$ is separated into N subinterval $[x_k, x_{k+1}](k = 0, 1, \ldots, N-1)$, $h = {}^{b-a}/_{N}$. Linear interpolation is used in each subinterval as shown in Fig. 2.16, then we get:

$$I_k = \int_{x_k}^{x_{k+1}} f(x)dx \approx \frac{h}{2}[f(x_k) + f(x_{k+1})]$$

Thus:

$$I = \int_a^b f(x)dx = \sum_{k=0}^{N-1} I_k = \frac{h}{2}\left[f(x_0) + \sum_{k=1}^{N-1} f(x_k) + f(x_k)\right] \tag{2.39}$$

Eq. (2.39) is the trapezoid formula in linear interpolation.

We separate the integrating range $[0, L]$ of Eq. (2.38) into N segment, so the length of each segment is $h = {}^{L}/_{N}$. Then, when $s = ih, \sigma = jh(i, j = 0, 1, \ldots, N)$, we get:

$$\hat{G}_{ij} = \begin{cases} \dfrac{m_A}{\rho} + L - ih & 0 \le j \le i \\ \dfrac{m_A}{\rho} + L - jh & i \le j \le N \end{cases}$$

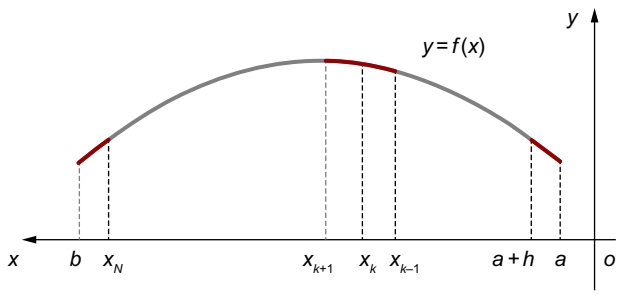

Fig. 2.16 Linear interpolation.

When $s=ih$, trapezoid formula is used for left of Eq. (3.1), we get:

$$\int_0^L \hat{G}\{[(1+\varepsilon)\boldsymbol{\tau}]^{\cdot\cdot}+\boldsymbol{q}\}$$

$$d\sigma \approx \frac{h}{2}\left[\left(\frac{m_A}{\rho}+L-ih\right)\boldsymbol{x}(j)+2\sum_{j=1}^{i}\left(\frac{m_A}{\rho}+L-ih\right)\boldsymbol{x}(j)\right.$$

$$\left.+2\sum_{j=i+1}^{N-1}\left(\frac{m_A}{\rho}+L-jh\right)\boldsymbol{x}(j)+\left(\frac{m_A}{\rho}+L-Nh\right)\boldsymbol{x}(N)\right]$$

where:

$$\boldsymbol{x}(j)=\{[1+\varepsilon(jh)]\boldsymbol{\tau}(jh)\}^{\cdot\cdot}+\boldsymbol{q}(jh)\quad(j=0,1,2,\ldots,N)$$

Similarly, trapezoid formula is used in right of Eq. (2.38), we get:

$$\frac{\boldsymbol{F}}{\rho}+\int_s^L\frac{\boldsymbol{f}}{\rho}d\sigma-\frac{\boldsymbol{n}(s)}{\rho}\approx\boldsymbol{y}(i)\triangleq\frac{\boldsymbol{F}-\boldsymbol{n}(ih)}{\rho}+\frac{h}{2\rho}\left[\boldsymbol{f}(ih)+2\sum_{j=i+1}^{N-1}\boldsymbol{f}(jh)+\boldsymbol{f}(Nh)\right]$$

When i is 0, 1, …, N respectively, Eq. (2.38) can be written into $N+1$ equation, and these $N+1$ equations can be rewritten into matrix formulations as:

$$[\boldsymbol{M}]_{(N+1)\times(N+1)}[\boldsymbol{x}]_{(N+1)\times1}=[\boldsymbol{y}]_{(N+1)\times1}$$

where:

$$\boldsymbol{M}=\frac{h}{2}\left[\begin{array}{c|ccccc|c}\hat{G}_{00} & 2\hat{G}_{01} & \cdots & 2\hat{G}_{0j} & \cdots & 2\hat{G}_{0(N-1)} & \hat{G}_{0N}\\ \vdots & \vdots & & \vdots & & \vdots & \vdots\\ \hat{G}_{i0} & 2\hat{G}_{i1} & \cdots & 2\hat{G}_{ij} & \cdots & 2\hat{G}_{i(N-1)} & \hat{G}_{iN}\\ \vdots & \vdots & & \vdots & & \vdots & \vdots\\ \hat{G}_{N0} & 2\hat{G}_{N1} & \cdots & 2\hat{G}_{Nj} & \cdots & 2\hat{G}_{N(N-1)} & \hat{G}_{NN}\end{array}\right]_{(N+1)\times(N+1)}$$

$$=\frac{h^2}{2}\begin{bmatrix}a+k & 2(a+k-1) & 2(a+k-2) & \cdots & a\\ a+k-1 & 2(a+k-1) & 2(a+k-2) & \cdots & a\\ a+k-2 & 2(a+k-2) & 2(a+k-2) & \cdots & a\\ \vdots & \vdots & \vdots & \ddots & \vdots\\ a & 2a & 2a & \cdots & a\end{bmatrix}$$

where $a=\frac{m_A}{\rho h}$.

The solution of the above equation is:

$$\boldsymbol{x} = \boldsymbol{M}^{-1}\boldsymbol{y}$$

The inverse matrix of $\boldsymbol{M}$ is satisfied with:

$$\boldsymbol{M}^{-1} = \frac{1}{h^2}\begin{bmatrix} 2 & -2 & & & & & & \\ -1 & 2 & -1 & & & & & \\ & -1 & 2 & -1 & & & & \\ & & \ddots & \ddots & \ddots & & & \\ & & & -1 & 2 & -1 & & \\ & & & & -1 & 2 & -1 & \\ & & & & & -2 & \dfrac{2(a+1)}{a} & \end{bmatrix}_{(N+1)\times(N+1)}$$

Expand the matrix equation, and introduce new variable $\boldsymbol{w}_j (j = 0, 1, \ldots, N)$, we get:

- When $j = 0$,

$$\boldsymbol{w}_0 \triangleq [(1+\varepsilon_0)\boldsymbol{\tau}_0]^{\cdot\cdot} = \frac{2}{\rho h^2}(\boldsymbol{n}_1 - \boldsymbol{n}_0) + \frac{\boldsymbol{f}_0 + \boldsymbol{f}_1}{\rho h} - \boldsymbol{q}_0 \tag{2.40}$$

- When $j = 1, 2, \ldots, N-1$,

$$\boldsymbol{w}_j \triangleq \left[\left(1+\varepsilon_j\right)\boldsymbol{\tau}_j\right]^{\cdot\cdot} = \frac{1}{\rho h^2}\left(\boldsymbol{n}_{j+1} - 2\boldsymbol{n}_j + \boldsymbol{n}_{j-1}\right) + \frac{\boldsymbol{f}_{j+1} - \boldsymbol{f}_{j-1}}{2\rho h} - \boldsymbol{q}_j \tag{2.41}$$

- When $j = N$,

$$\boldsymbol{w}_N \triangleq [(1+\varepsilon_N)\boldsymbol{\tau}_N]^{\cdot\cdot} = -\frac{2}{\rho h^2}(\boldsymbol{n}_N - \boldsymbol{n}_{N-1}) - \frac{2\boldsymbol{n}_N}{m_A h} - \frac{\boldsymbol{f}_{N-1} + \boldsymbol{f}_N}{\rho h} + \frac{2\boldsymbol{F}}{h m_A} - \boldsymbol{q}_N \tag{2.42}$$

Half discretization is done through this set of equations. It is easier to be used for numerical process compared to the method mentioned in the reference, since it has both motion equations and boundary conditions.

There are different descriptions to describe the unit tangent vector in three dimensions, in which a conventional method is that two angles are

used to describe it. But this method may lead to system singular. So we use unit tangent vector with respect to Cartesian coordinate:

$$\boldsymbol{\tau}_j = \begin{bmatrix} \tau_{xj} \\ \tau_{yj} \\ \tau_{zj} \end{bmatrix}, \quad \text{and} \quad \boldsymbol{\tau}_j \cdot \boldsymbol{\tau}_j = \tau_{xj}^2 + \tau_{yj}^2 + \tau_{zj}^2 = 1$$

while:

$$\boldsymbol{w}_j = \left[\left(1+\varepsilon_j\right)\boldsymbol{\tau}_j\right]^{\cdot\cdot} = \ddot{\varepsilon}_j\boldsymbol{\tau}_j + \dot{\varepsilon}_j\dot{\boldsymbol{\tau}}_j + \left(1+\varepsilon_j\right)\ddot{\boldsymbol{\tau}}_j$$

So we get:

$$\begin{bmatrix} \left(1+\varepsilon_j\right)\boldsymbol{\tau}_j \\ \dfrac{\boldsymbol{\tau}_j \cdot \boldsymbol{\tau}_j}{2} \end{bmatrix}^{\cdot\cdot} = \begin{bmatrix} w_{xj} \\ w_{yj} \\ w_{zj} \\ 0 \end{bmatrix} = \begin{bmatrix} 1+\varepsilon_j & 0 & 0 & \tau_{xj} \\ 0 & 1+\varepsilon_j & 0 & \tau_{yj} \\ 0 & 0 & 1+\varepsilon_j & \tau_{zj} \\ \tau_{xj} & \tau_{yj} & \tau_{zj} & 0 \end{bmatrix} \begin{bmatrix} \ddot{\tau}_{xj} \\ \ddot{\tau}_{yj} \\ \ddot{\tau}_{zj} \\ \ddot{\varepsilon}_j \end{bmatrix} + \begin{bmatrix} 2\dot{\varepsilon}_j\dot{\tau}_{xj} \\ 2\dot{\varepsilon}_j\dot{\tau}_{yj} \\ 2\dot{\varepsilon}_j\dot{\tau}_{zj} \\ \dot{\tau}_{xj}^2 + \dot{\tau}_{yj}^2 + \dot{\tau}_{zj}^2 \end{bmatrix}$$

then:

$$\begin{bmatrix} \ddot{\tau}_{xj} \\ \ddot{\tau}_{yj} \\ \ddot{\tau}_{zj} \\ \ddot{\varepsilon}_j \end{bmatrix} = \frac{1}{1+\varepsilon_j} \begin{bmatrix} \tau_{yj}^2 + \tau_{zj}^2 & -\tau_{xj}\tau_{yj} & -\tau_{xj}\tau_{zj} & \left(1+\varepsilon_j\right)\tau_{xj} \\ -\tau_{xj}\tau_{yj} & \tau_{xj}^2 + \tau_{zj}^2 & -\tau_{yj}\tau_{zj} & \left(1+\varepsilon_j\right)\tau_{yj} \\ -\tau_{xj}\tau_{zj} & -\tau_{yj}\tau_{zj} & \tau_{xj}^2 + \tau_{yj}^2 & \left(1+\varepsilon_j\right)\tau_{zj} \\ \left(1+\varepsilon_j\right)\tau_{xj} & \left(1+\varepsilon_j\right)\tau_{yj} & \left(1+\varepsilon_j\right)\tau_{zj} & -\left(1+\varepsilon_j\right)^2 \end{bmatrix} \begin{bmatrix} w_{xj} - 2\dot{\varepsilon}_j\dot{\tau}_{xj} \\ w_{yj} - 2\dot{\varepsilon}_j\dot{\tau}_{yj} \\ w_{zj} - 2\dot{\varepsilon}_j\dot{\tau}_{zj} \\ -\left(\dot{\tau}_{xj}^2 + \dot{\tau}_{yj}^2 + \dot{\tau}_{zj}^2\right) \end{bmatrix} \tag{2.43}$$

Eqs. (2.19), (2.40)–(2.43) consist of the discretization of the Sapce Tethered Robotic System during the station-keeping phase. It is not only a discretization of the equations of dynamics, but also a separation of the axial motion and lateral motion, which makes the solution of ill-condition system much easier. Since it is the function of time t, normal numerical

integration algorithm such as Euler, Runge-Kutta, and Gill can be used for calculation.

We derive the dynamics model composed of Eqs. (2.17)–(2.19), (2.31)–(2.34), and (2.36). Since the length of the tether varies constantly during the deployment and retrieval, the definition domain of Eq. (2.31) changes constantly, which leads to the previous method of discretization useless in this case. So we improve the method of discretization.

According to Eq. (2.17), (2.18), and (2.32), we get:

$$\boldsymbol{r}(s,t) = \boldsymbol{r}_D + \int_{\xi}^{L} (1+\varepsilon)\boldsymbol{\tau} d\sigma$$

then:

$$\dot{\boldsymbol{r}}(s,t) = \int_{\xi}^{s} [(1+\varepsilon)\boldsymbol{\tau}]^{\cdot} d\sigma - [1+\varepsilon(\xi)]\boldsymbol{\tau}(\xi)\dot{\xi}$$

$$\ddot{\boldsymbol{r}}(s,t) = \int_{\xi}^{s} [(1+\varepsilon)\boldsymbol{\tau}]^{\cdot\cdot} d\sigma - 2\{[1+\varepsilon(\xi)]\boldsymbol{\tau}(\xi)\}^{\cdot}\dot{\xi} - [1+\varepsilon(\xi)]\boldsymbol{\tau}(\xi)\ddot{\xi}$$

$$\boldsymbol{p}(s,t) = \int_{\xi}^{s} \boldsymbol{q}(s,t) d\sigma - 2\boldsymbol{\omega} \times \{[1+\varepsilon(\xi)]\boldsymbol{\tau}(\xi)\}\dot{\xi} + \boldsymbol{c}(t)$$

where:

$$\boldsymbol{c}(t) = \dot{\boldsymbol{\omega}}(t) \times \boldsymbol{r}_D + \boldsymbol{\omega}(t) \times [\boldsymbol{\omega}(t) \times \boldsymbol{r}_D] + \mu_e \left[\frac{\boldsymbol{r}_D}{R_B^3} - 3(\boldsymbol{r}_D \cdot \boldsymbol{R}_B)\frac{\boldsymbol{R}_B}{R_B^5} \right] \tag{2.44}$$

thus:

$$\begin{aligned} \int_{s}^{L} (\ddot{\boldsymbol{r}} + \boldsymbol{p}) d\sigma &= (\ddot{\boldsymbol{r}} + \boldsymbol{p})\sigma|_{s}^{L} - \int_{s}^{L} (\ddot{\boldsymbol{r}}' + \boldsymbol{p}')\sigma d\sigma \\ &= [\ddot{\boldsymbol{r}}(L) + \boldsymbol{p}(L)]L - [\ddot{\boldsymbol{r}}(s) + \boldsymbol{p}(s)]s - \int_{s}^{L} \{[(1+\varepsilon)\boldsymbol{\tau}]^{\cdot\cdot} + \boldsymbol{q}\}\sigma d\sigma \\ &= \int_{\xi}^{L} G\{[(1+\varepsilon)\boldsymbol{\tau}]^{\cdot\cdot} + \boldsymbol{q}\} d\sigma - \boldsymbol{g}(L-s) \end{aligned}$$

where g is the equivalent acceleration caused by tether length:

$$\boldsymbol{g} = 2\boldsymbol{\omega} \times \{[1+\varepsilon(\xi)]\boldsymbol{\tau}(\xi)\}\dot{\xi} + 2\{[1+\varepsilon(\xi)]\boldsymbol{\tau}(\xi)\}^{\cdot}\dot{\xi} + [1+\varepsilon(\xi)]\boldsymbol{\tau}(\xi)\ddot{\xi} - \boldsymbol{c}(t) \tag{2.45}$$

Integrate Eq. (2.31):

$$\int_{\xi}^{L} G\{[(1+\varepsilon)\boldsymbol{\tau}]^{\cdot\cdot} + \boldsymbol{q}\}d\sigma = \frac{1}{\rho}[\boldsymbol{n}(L) - \boldsymbol{n}(s)] + \int_{s}^{L}\frac{\boldsymbol{f}}{\rho}d\sigma + \boldsymbol{g}(L-s)$$

Substitute the boundary condition (2.33) into the above integration equation:

$$\int_{\xi}^{L} \hat{G}\{[(1+\varepsilon)\boldsymbol{\tau}]^{\cdot\cdot} + \boldsymbol{q}\}d\sigma = \boldsymbol{g}\left(\frac{m_A}{\rho} + L - s\right) + \frac{\boldsymbol{F}}{\rho} + \int_{s}^{L}\frac{\boldsymbol{f}}{\rho}d\sigma - \frac{\boldsymbol{n}(s)}{\rho} \tag{2.46}$$

Due to the equivalent acceleration, integration equation of deployment and retrieval (2.46) is similar to Eq. (2.38). But because the integration range of Eq. (2.46) varies constantly, it is difficult to discrete.

For discretization of Eq. (2.46), we separate the integration range $[\xi, L]$ into N segments as shown in Fig. 2.17, where the length of first segment is η,

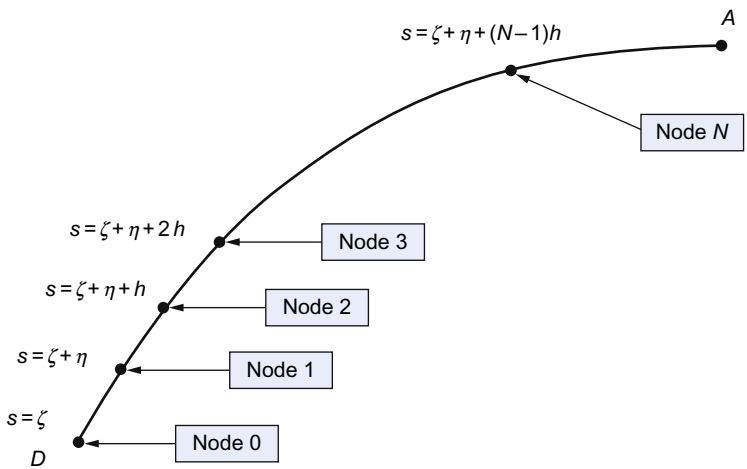

Fig. 2.17 Tether segments.

and others are h. A similar partial linear interpolation is used as mentioned in Section 2.3. So we get:

$$\int_{\xi}^{L}\hat{G}\{[(1+\varepsilon)\boldsymbol{\tau}]^{\cdot\cdot}+\boldsymbol{q}\}d\sigma=\int_{\xi}^{\xi+\eta}\hat{G}\{[(1+\varepsilon)\boldsymbol{\tau}]^{\cdot\cdot}+\boldsymbol{q}\}d\sigma+\int_{\xi+\eta}^{L}\hat{G}\{[(1+\varepsilon)\boldsymbol{\tau}]^{\cdot\cdot}+\boldsymbol{q}\}d\sigma$$

$$\int_{\xi}^{\xi+\eta}\hat{G}\{[(1+\varepsilon)\boldsymbol{\tau}]^{\cdot\cdot}+\boldsymbol{q}\}d\sigma\approx\frac{\eta}{2}\left[\hat{G}_{i0}\boldsymbol{x}(0)+\hat{G}_{i1}\boldsymbol{x}(1)\right]\int_{\xi+\eta}^{L}\hat{G}\{[(1+\varepsilon)\boldsymbol{\tau}]^{\cdot\cdot}+\boldsymbol{q}\}d\sigma$$

$$\approx\frac{h}{2}\left[\hat{G}_{i1}\boldsymbol{x}(1)+\sum_{j=2}^{N-1}\hat{G}_{ij}\boldsymbol{x}(j)+\hat{G}_{iN}\boldsymbol{x}(N)\right]$$

where i and j are the sequence numbers of nodes, such as $\hat{G}_{34}$ denotes $\hat{G}$ when $\sigma=\xi+\eta+3h$, and $\boldsymbol{x}(5)$ denotes $[(1+\varepsilon)\boldsymbol{\tau}]^{\cdot\cdot}+\boldsymbol{q}$ of the node 5. The same method is used for the integration of the right hand of Eq. (3.9), then we get:

$$\boldsymbol{g}\left(\frac{m_A}{\rho}+L-s\right)+\frac{\boldsymbol{F}}{\rho}+\int_{s}^{L}\frac{\boldsymbol{f}}{\rho}d\sigma-\frac{\boldsymbol{n}(s)}{\rho}\approx$$

$$\boldsymbol{y}(i)\triangleq\begin{cases}\dfrac{\boldsymbol{F}-\boldsymbol{n}_0}{\rho}+\dfrac{h}{2\rho}\left(\boldsymbol{f}_1+2\sum_{j=2}^{N-1}\boldsymbol{f}_j+\boldsymbol{f}_N\right)+\dfrac{\eta}{2\rho}(\boldsymbol{f}_0+\boldsymbol{f}_1)+\dfrac{m_A}{\rho}\boldsymbol{g} & i=0\\ \dfrac{\boldsymbol{F}-\boldsymbol{n}_i}{\rho}+\dfrac{h}{2\rho}\left(\boldsymbol{f}_i+2\sum_{j=i+1}^{N-1}\boldsymbol{f}_j+\boldsymbol{f}_N\right)+\left[\dfrac{m_A}{\rho}+L-\xi-\eta-(i-1)h\right]\boldsymbol{g} & i>0\end{cases}$$

Similarly as the discretization in station-keeping phase, when i is 0,1,…, N respectively, Eq. (2.46) can be write in $N+1$ equations, which can be rewrite in matrix as:

$$\left[\hat{\boldsymbol{M}}\right]_{(N+1)\times(N+1)}[\boldsymbol{x}]_{(N+1)\times1}=[\boldsymbol{y}]_{(N+1)\times1}$$

where:

$$\hat{\boldsymbol{M}}=\left[\begin{array}{c|c|ccccc|c}
\frac{\eta}{2}\hat{G}_{00} & \frac{h+\eta}{2}\hat{G}_{01} & h\hat{G}_{02} & \cdots & h\hat{G}_{0j} & \cdots & h\hat{G}_{0(N-1)} & \frac{h}{2}\hat{G}_{0N} \\
\vdots & \vdots & \vdots & & \vdots & & \vdots & \vdots \\
\frac{\eta}{2}\hat{G}_{10} & \frac{h+\eta}{2}\hat{G}_{11} & h\hat{G}_{12} & \cdots & h\hat{G}_{ij} & \cdots & h\hat{G}_{i(N-1)} & \frac{h}{2}\hat{G}_{iN} \\
\vdots & \vdots & \vdots & & \vdots & & \vdots & \vdots \\
\frac{\eta}{2}\hat{G}_{N0} & \frac{h+\eta}{2}\hat{G}_{N1} & h\hat{G}_{N2} & \cdots & h\hat{G}_{Ni} & \cdots & h\hat{G}_{N(N-1)} & \frac{h}{2}\hat{G}_{NN}
\end{array}\right]_{(N+1)\times(N+1)}$$

The inverse matrix of $\hat{\boldsymbol{M}}$ fulfills:

$$\hat{\boldsymbol{M}}^{-1}=\frac{1}{h^2}\begin{bmatrix}
\frac{2h^2}{\eta^2} & -\frac{2h^2}{\eta^2} & & & & & & \\
-\frac{2h^2}{\eta(\eta+h)} & \frac{2h}{\eta} & -\frac{2h}{\eta+h} & & & & & \\
 & -1 & 2 & -1 & & & & \\
 & & \ddots & \ddots & \ddots & & & \\
 & & & -1 & 2 & -1 & & \\
 & & & & -1 & 2 & -1 & \\
 & & & & & -2 & \frac{2(m_A+\rho h)}{m_A}
\end{bmatrix}_{(N+1)\times(N+1)}$$

Expand the solution of matrix:

- When $j=0$,

$$\boldsymbol{w}_0=\left[(1+\varepsilon_0)\boldsymbol{\tau}_0\right]^{\cdot\cdot}=\frac{2}{\eta}\boldsymbol{g}+\frac{2}{\rho\eta^2}(\boldsymbol{n}_1-\boldsymbol{n}_0)+\frac{\boldsymbol{f}_0+\boldsymbol{f}_1}{\rho\eta}-\boldsymbol{q}_0 \tag{2.47}$$

- When $j=1$,

$$\begin{aligned}\boldsymbol{w}_1&=\left[(1+\varepsilon_1)\boldsymbol{\tau}_1\right]^{\cdot\cdot}\\&=\frac{2}{\rho\eta(h+\eta)}(\boldsymbol{n}_0-\boldsymbol{n}_1)+\frac{2}{\rho h(h+\eta)}(\boldsymbol{n}_2-\boldsymbol{n}_1)+\frac{\boldsymbol{f}_2-\boldsymbol{f}_0}{\rho(h+\eta)}-\boldsymbol{q}_1\end{aligned} \tag{2.48}$$

- When $j=2,\ldots,N-1$,

$$\boldsymbol{w}_j\triangleq\left[\left(1+\varepsilon_j\right)\boldsymbol{\tau}_j\right]^{\cdot\cdot}=\frac{1}{\rho h^2}\left(\boldsymbol{n}_{j+1}-2\boldsymbol{n}_j+\boldsymbol{n}_{j-1}\right)+\frac{\boldsymbol{f}_{j+1}-\boldsymbol{f}_{j-1}}{2\rho h}-\boldsymbol{q}_j \tag{2.49}$$

- When $j=N$,

$$\boldsymbol{w}_N \triangleq [(1+\varepsilon_N)\boldsymbol{\tau}_N]^{\cdot\cdot} = -\frac{2}{\rho h^2}(\boldsymbol{n}_N - \boldsymbol{n}_{N-1}) - \frac{2\boldsymbol{n}_N}{m_A h} - \frac{\boldsymbol{f}_{N-1}+\boldsymbol{f}_N}{\rho h} + \frac{2\boldsymbol{F}}{h m_A} - \boldsymbol{q}_N \tag{2.50}$$

Eqs. (2.47)–(2.50) accomplish the discretization of mathematical model during deployment and retrieval. Eqs. (2.19), (2.33), (2.34), (2.47)–(2.50), and (2.43) form a closed-system. ξ changes constantly in deployment and retrieval, and for the assurance of:

$$\xi + \eta + (N-1)h = L \tag{2.51}$$

Further improvement are required.

During the deployment and retrieval of flexible tether, we defined segment length h as constant, which compensate the variable of ξ in Eq. (3.15), and then η changes as ξ in a small range. The system will be singular when η oversize or undersize, which leads to the failure solution of the equations. Thus, we define η as:

$$0.5h \le \eta < 1.5h \tag{2.52}$$

To prove this definition, we study it in two cases:

(1) When $\eta \ge 1.5h$, we insert a new node between node 0 and 1, and the natural length between new node and node 1 is h, as shown in Fig. 2.18. The sates of the new node is acquired via linear interpolation as:

$$\varepsilon_* = \frac{h}{\eta}\varepsilon_0 + \frac{\eta-h}{\eta}\varepsilon_1,\ \boldsymbol{\tau}_* = \frac{h}{\eta}\boldsymbol{\tau}_0 + \frac{\eta-h}{\eta}\boldsymbol{\tau}_1,$$
$$\dot{\varepsilon}_* = \frac{h}{\eta}\dot{\varepsilon}_0 + \frac{\eta-h}{\eta}\dot{\varepsilon}_1,\ \dot{\boldsymbol{\tau}}_* = \frac{h}{\eta}\dot{\boldsymbol{\tau}}_0 + \frac{\eta-h}{\eta}\dot{\boldsymbol{\tau}}_1,$$

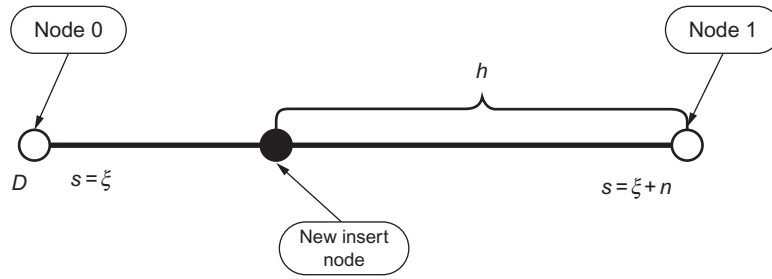

Fig. 2.18 Insertion of the new node.

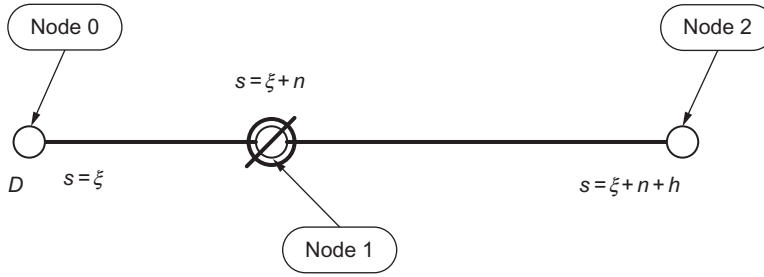

Fig. 2.19 Deletion of the node.

The total number of nodes becomes $N+1$ when new node is inserted, and $\eta^* = \eta - h \in [0.5h, 1.5h)$.

(2) When $\eta < 0.5h$, we combine the first and second tether segment, and delete node 1, as shown in Fig. 2.19. Then the total number of nodes becomes $N-1$, and $\eta^* = \eta + h \in [0.5h, 1.5h)$.

Eq. (2.51) is proved through deletion and insertion of node. In addition, compared to the Bead model by treating the segment between the release point and the first node (anchor point) as a rigid link, the continuity is ensured and the error is reduced through the linear interpolation of new node.

2.5 DYNAMICS MODELING AND SOLVING BASED ON HAMILTONIAN

The assumptions of the dynamics model based on the Euler method are too rigorous and the discretization is too simple. To analyze the space tether accurately, we use the Hamiltonian method for the dynamics model of the system, and the finite element method for the discretization. First, similarly as the previous section, the attitude motion of terminal capture device in Fig. 2.1 is ignored, and the platform satellite and operational robot are treated as mass points. The tether is simplified as a line segment by ignoring torsional stiffness and bending stiffness of tether. The simplified configuration of the system is shown in Fig. 2.20. In addition, the Earth-Equator inertial coordinate system is defined to describe the three-dimensional motion of the TSRS, who has origin O at the center of Earth, X-axis along the line of intersection of equatorial plane and ecliptic plane and towards vernal point, Z-axis towards the North Pole, Y-axis normal to X-axis in the equatorial plane. Orbit coordinate system $oxyz$ is defined as that origin o is around the system and working on the circular Keplerian orbit which is not accepted by the TSRS. oxz plane is the orbit plane of the motion of

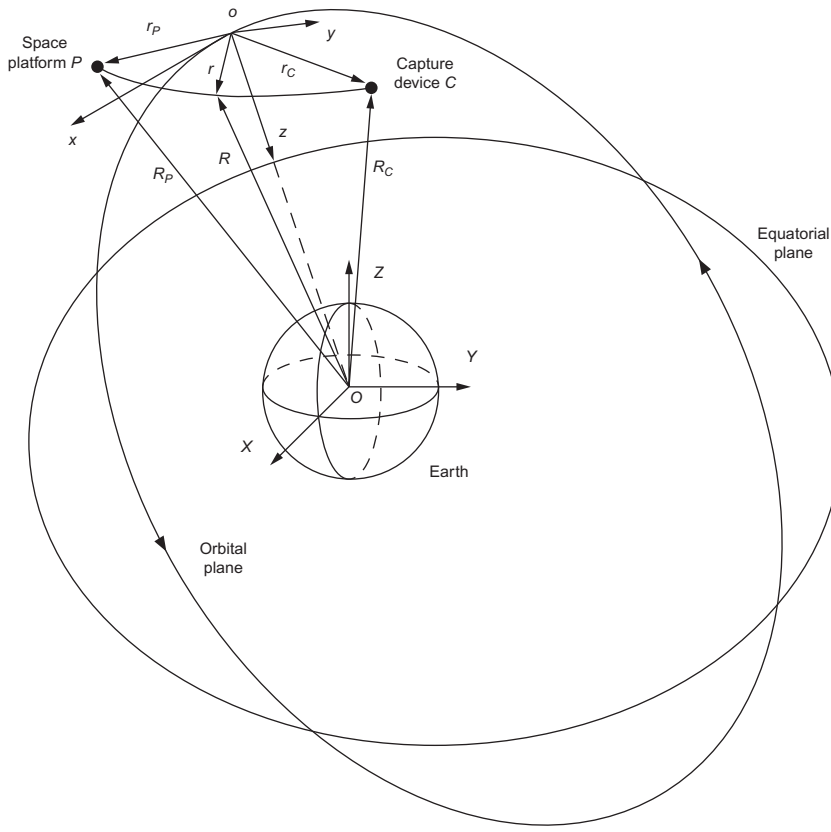

Fig. 2.20 Simple configuration of the TSRS.

origin o, with x-axis along orbit tangential and towards motion direction of origin o, and with z-axis coinciding to the line between origin o and center of Earth O, towards center of Earth. y-axis is opposite along the normal of orbit plane.

Since the capstan mechanism is not easy for the dynamics analysis during deployment/retrieval, a simple model is addressed in this section as shown in Fig. 2.21, where the storage tether in the platform is released under the tension $N(\xi)$, and retrieved under the tension N_P. Because the tether infinitesimal is accelerated or moderated instantly during the deployment and retrieval, only the conservation of momentum but not the conservation of mechanical energy is satisfied in these two cases, which makes it much more difficult to analyze the dynamics. Crellin et al. [14] proposed the Carnot energy loss term (CELT) to fix the energy equation of the system, which can ensure the correctness of model. The result in the reference is used

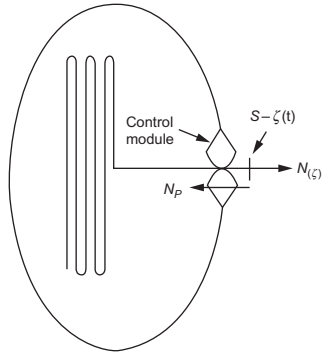

Fig. 2.21 Schematic of deployment/retrieval mechanism.

directly in this section when the Hamilton variation is used for dynamics analysis.

For space tether, Kelvin-Voigt is generally used as the linear model of tension which is expressed as:

$$N = N_C + N_D = EA(\varepsilon + \alpha\dot{\varepsilon}) \tag{2.53}$$

where N is the magnitude of the tension of the tether, N_C and N_D are the elastic force and damping force of the tether respectively, ε is the deformation of the tether, $\dot{\varepsilon}$ is the deformation rate of the tether, E is the Yong's module of the tether, A is the cross-sectional area of the tether, and α is the damping coefficient of the tether. According to the high stiffness of material used as a space tether, false compression stress generates when the tether is slack, which leads to strong oscillation in the simulation. This strong oscillation may lead to divergence, which departs from the practical condition of the tether motion.

To solve this problem, motion of the space tether under the tension is analyzed in the reference. When the tether is under pressure, only small stiffness occurs because fibers have low compression ability. The fibers will be tight and appear stiff only when the tension is large enough. To describe this characteristic of the tether, a stress-strain equation is introduced in this section:

$$\sigma = \frac{1}{2}E\left[(\varepsilon - \varepsilon_0) + \sqrt{(\varepsilon - \varepsilon_0)^2 + 4\left(\frac{T_0}{EA}\right)^2}\right] \tag{2.54}$$

where σ is the strain of the tether, ε_0 is the initial strain of tether, T_0 is the initial axial force of tether. Thus the elastic force N_C under the nonlinear condition fulfills:

$$N_C = \frac{1}{2}EA\left[(\varepsilon-\varepsilon_0)+\sqrt{(\varepsilon-\varepsilon_0)^2+4\left(\frac{T_0}{EA}\right)^2}\right] \tag{2.55}$$

Substitute the elastic terms in Eq. (2.53) by (2.55):

$$N = N_C + N_D = \frac{1}{2}EA\left[(\varepsilon-\varepsilon_0)+\sqrt{(\varepsilon-\varepsilon_0)^2+4\left(\frac{T_0}{EA}\right)^2}+2\alpha\dot{\varepsilon}\right] \tag{2.56}$$

The TSRS is composed of a released tether, a platform satellite, a storage tether, and a terminal capture device. The kinetic energy of the system is:

$$T = \int_{\xi}^{L}\frac{1}{2}\mu\dot{\boldsymbol{R}}^2\mathrm{d}s+\frac{1}{2}m_{\mathrm{P}}\dot{\boldsymbol{R}}_{\mathrm{P}}^2+\frac{1}{2}\mu\xi\dot{\boldsymbol{R}}_{\mathrm{P}}^2+\frac{1}{2}m_{\mathrm{C}}\dot{\boldsymbol{R}}_{\mathrm{C}}^2 \tag{2.57}$$

where μ is the density of tether, m_{P} and m_{C} are the masses of platform and terminal device respectively, $()^{\bullet}$ is the time derivative. The potential energy of the system is:

$$V = \int_{\xi}^{L}\left(\Pi-\mu\frac{GM}{|\boldsymbol{R}|}\right)\mathrm{d}s-m_{\mathrm{P}}\frac{GM}{|\boldsymbol{R}_{\mathrm{P}}|}-\mu\xi\frac{GM}{|\boldsymbol{R}_{\mathrm{P}}|}-m_{\mathrm{C}}\frac{GM}{|\boldsymbol{R}_{\mathrm{C}}|} \tag{2.58}$$

where G is the constant of universal gravitation, M the mass of Earth, Π is the potential energy which is expressed as:

$$\Pi = \int_{0}^{\varepsilon}N_C(\varepsilon)\mathrm{d}\varepsilon \tag{2.59}$$

The nonconservative forces of this system are the damping force of the tether, the control forces for the platform and the terminal device during deployment/retrieval. Thus the virtual work of nonconservative forces is:

$$\delta' W = \int_{\xi}^{L}-N_D\delta\varepsilon\mathrm{d}s+\boldsymbol{F}_{\mathrm{P}}\cdot\delta\boldsymbol{r}_{\mathrm{P}}+\boldsymbol{F}_{\mathrm{C}}\cdot\delta\boldsymbol{r}_{\mathrm{C}}+N_{\mathrm{P}}\eta(\xi)\delta\xi+\mathrm{CELT} \tag{2.60}$$

where $\boldsymbol{F}_{\mathrm{P}}$ and $\boldsymbol{F}_{\mathrm{C}}$ are control forces on the platform and terminal device respectively, $\eta(\xi)=1+\varepsilon(\xi)$, CELT is:

$$\mathrm{CELT}=\begin{cases}\dfrac{1}{2}\mu\dot{\xi}^2\eta^2(\xi)-\Pi(\xi) & \dot{\xi}\le 0\\ -\dfrac{1}{2}\mu\dot{\xi}^2\eta(\xi)(2-\eta(\xi))-\Pi(\xi) & \dot{\xi}>0\end{cases} \tag{2.61}$$

where $\dot{\xi}\le 0$ means to deployment, and $\dot{\xi}>0$ means to retrieval.

According to the Hamilton variation, the motion equation of the system is:

$$\int_0^t(\delta T-\delta V+\delta' W)\mathrm{d}t=0 \tag{2.62}$$

where δ is the variation calculation. Thus Eq. (2.57) is written after the variation calculation as:

$$\begin{aligned}\delta T=&\int_\xi^L\mu\dot{\boldsymbol{R}}\delta\dot{\boldsymbol{R}}\mathrm{d}s\\&-\frac{1}{2}\mu\dot{\boldsymbol{R}}^2\big|_{s=\xi}\delta\xi+m_{\mathrm{P}}\dot{\boldsymbol{R}}_{\mathrm{P}}\delta\dot{\boldsymbol{R}}_{\mathrm{P}}+m_{\mathrm{C}}\dot{\boldsymbol{R}}_{\mathrm{C}}\delta\dot{\boldsymbol{R}}_{\mathrm{C}}+\mu\xi\dot{\boldsymbol{R}}_{\mathrm{P}}\delta\dot{\boldsymbol{R}}_{\mathrm{P}}+\frac{1}{2}\mu\dot{\boldsymbol{R}}_{\mathrm{P}}^2\delta\xi\end{aligned} \tag{2.63}$$

Integrate the first term of Eq. (2.63):

$$\begin{aligned}&\int_0^t\int_\xi^L\mu\dot{\boldsymbol{R}}\delta\dot{\boldsymbol{R}}\mathrm{d}s\mathrm{d}t=\int_0^t\int_\xi^L\left[\frac{\mathrm{d}}{\mathrm{d}t}\left(\mu\dot{\boldsymbol{R}}\delta\boldsymbol{R}\right)-\mu\ddot{\boldsymbol{R}}\delta\boldsymbol{R}\right]\mathrm{d}s\mathrm{d}t\\&=\int_0^t\int_\xi^L\frac{\mathrm{d}}{\mathrm{d}t}\left(\mu\dot{\boldsymbol{R}}\delta\boldsymbol{R}\right)\mathrm{d}s\mathrm{d}t-\int_0^t\int_\xi^L\mu\ddot{\boldsymbol{R}}\delta\boldsymbol{R}\mathrm{d}s\mathrm{d}t\\&=\int_0^t\left[\frac{\mathrm{d}}{\mathrm{d}t}\left(\int_\xi^L\mu\dot{\boldsymbol{R}}\delta\boldsymbol{R}\mathrm{d}s\right)+\mu\dot{\boldsymbol{R}}\dot{\xi}\delta\boldsymbol{R}\big|_{s=\xi}\right]\mathrm{d}t-\int_0^t\int_\xi^L\mu\ddot{\boldsymbol{R}}\delta\boldsymbol{R}\mathrm{d}s\mathrm{d}t=\int_\xi^L\mu\dot{\boldsymbol{R}}\delta\boldsymbol{R}\mathrm{d}s\Big|_0^t\\&+\int_0^t\mu\dot{\boldsymbol{R}}\dot{\xi}\delta\boldsymbol{R}\big|_{s=\xi}\mathrm{d}t-\int_0^t\int_\xi^L\mu\ddot{\boldsymbol{R}}\delta\boldsymbol{R}\mathrm{d}s\mathrm{d}t=\int_0^t\mu\dot{\boldsymbol{R}}\dot{\xi}\delta\boldsymbol{R}\big|_{s=\xi}\mathrm{d}t\\&-\int_0^t\int_\xi^L\mu\ddot{\boldsymbol{R}}\delta\boldsymbol{R}\mathrm{d}s\mathrm{d}t\end{aligned} \tag{2.64}$$

Do the same to the third, fourth, and fifth terms of the Eq. (2.63):

$$\begin{aligned}\int_0^t \delta T \mathrm{d}t \;=\; & \int_0^t \left[-\int_\xi^L \mu \ddot{\boldsymbol{R}} \delta \boldsymbol{R} \mathrm{d}s - m_\mathrm{P} \ddot{\boldsymbol{R}}_\mathrm{P} \delta \boldsymbol{R}_\mathrm{P} - \mu\xi \ddot{\boldsymbol{R}}_\mathrm{P} \delta \boldsymbol{R}_\mathrm{P} - m_\mathrm{C} \ddot{\boldsymbol{R}}_\mathrm{C} \delta \boldsymbol{R}_\mathrm{C} + \right. \\ & \left. -\frac{1}{2}\mu \dot{\boldsymbol{R}}^2 \Big|_{s=\xi} \delta\xi + \mu \dot{\boldsymbol{R}}\big|_{s=\xi} \dot{\xi} \delta \boldsymbol{R}|_{s=\xi} - \mu \dot{\xi} \dot{\boldsymbol{R}}_\mathrm{P} \delta \boldsymbol{R}_\mathrm{P} + \frac{1}{2}\mu \dot{\boldsymbol{R}}_\mathrm{P}^2 \delta\xi \right] \mathrm{d}t\end{aligned} \tag{2.65}$$

From the derivative of compound function, we get:

$$\frac{\mathrm{d}}{\mathrm{d}t}\boldsymbol{R}_\mathrm{P} = \frac{\mathrm{d}}{\mathrm{d}t}\boldsymbol{R}(\xi, t) = \dot{\xi}\frac{\partial \boldsymbol{R}(s,t)}{\partial s}\bigg|_{s=\xi} + \frac{\partial \boldsymbol{R}(s,t)}{\partial t}\bigg|_{s=\xi} = \eta(\xi)\dot{\xi}\boldsymbol{\tau}(\xi) + \dot{\boldsymbol{R}}\big|_{s=\xi} \tag{2.66}$$

$$\delta \boldsymbol{R}_\mathrm{P} = \eta(\xi)\boldsymbol{\tau}(\xi)\delta\xi + \delta \boldsymbol{R}|_{s=\xi} \tag{2.67}$$

Hence:

$$\begin{aligned} & -\frac{1}{2}\mu \dot{\boldsymbol{R}}^2 \Big|_{s=\xi} \delta\xi + \mu \dot{\boldsymbol{R}}\big|_{s=\xi} \dot{\xi} \delta \boldsymbol{R}|_{s=\xi} \\ & -\mu \dot{\xi} \dot{\boldsymbol{R}}_\mathrm{P} \delta \boldsymbol{R}_\mathrm{P} + \frac{1}{2}\mu \dot{\boldsymbol{R}}_\mathrm{P}^2 \delta\xi \\ & = \frac{1}{2}\mu \left(\dot{\boldsymbol{R}}_\mathrm{P} + \dot{\boldsymbol{R}}\big|_{s=\xi} \right) \eta(\xi)\dot{\xi}\boldsymbol{\tau}(\xi)\delta\xi + \mu \dot{\boldsymbol{R}}\big|_{s=\xi} \dot{\xi} \delta \boldsymbol{R}_\mathrm{P} \\ & -\mu \dot{\boldsymbol{R}}\big|_{s=\xi} \dot{\xi} \eta(\xi)\boldsymbol{\tau}(\xi)\delta\xi - \mu \dot{\xi} \dot{\boldsymbol{R}}_\mathrm{P} \delta \boldsymbol{R}_\mathrm{P} \\ & = \frac{1}{2}\eta^2(\xi)\dot{\xi}^2 \delta\xi \end{aligned} \tag{2.68}$$

Based on variation calculation of (2.58), we get:

$$\begin{aligned} \delta V = & \int_\xi^L \left(N_\mathrm{C}\delta\varepsilon + \mu \frac{GM}{|\boldsymbol{R}|^3}\boldsymbol{R} \cdot \delta \boldsymbol{R} \right) \mathrm{d}s - \Pi(\xi)\delta\xi + m_\mathrm{P}\frac{GM}{|\boldsymbol{R}_\mathrm{P}|^3}\boldsymbol{R}_\mathrm{P} \cdot \delta \boldsymbol{R}_\mathrm{P} \\ & + m_\mathrm{C}\frac{GM}{|\boldsymbol{R}_\mathrm{C}|^3}\boldsymbol{R}_\mathrm{C} \cdot \delta \boldsymbol{R}_\mathrm{C} + \mu\xi \frac{GM}{|\boldsymbol{R}_\mathrm{P}|^3}\boldsymbol{R}_\mathrm{P} \cdot \delta \boldsymbol{R}_\mathrm{P} \end{aligned} \tag{2.69}$$

From Eqs. (2.63)–(2.69), the equations of motion of the system during deployment are:

$$\begin{aligned}
&\int_0^t \Bigg\{ \int_\xi^L \left[-\mu \boldsymbol{A} + \frac{\partial \boldsymbol{n}}{\partial s} \right] \delta \boldsymbol{R} \mathrm{d}s \\
&+ \left[\mu \dot{\xi}^2 \eta^2(\xi) + N_\mathrm{P} \eta(\xi) - N(\xi) \eta(\xi) \right] \delta \xi \\
&+ \left[-(m_\mathrm{P} + \mu\xi) \boldsymbol{A}_\mathrm{P} - \mu \dot{\xi}^2 \frac{\partial \boldsymbol{R}(\xi)}{\partial s} + \boldsymbol{F}_\mathrm{P} + \boldsymbol{n}(\xi) \right] \delta \boldsymbol{R}_\mathrm{P} \\
&+ [-m_\mathrm{C} \boldsymbol{A}_\mathrm{C} + \boldsymbol{F}_\mathrm{C} - \boldsymbol{n}(L)] \delta \boldsymbol{R}_\mathrm{C} \Bigg\} \mathrm{d}t = 0
\end{aligned} \tag{2.70}$$

According the arbitrariness of variation, we get:

$$\begin{aligned}
G_D \triangleq &\int_\xi^L \left[-\mu \boldsymbol{A} + \frac{\partial \boldsymbol{n}}{\partial s} \right] \delta \boldsymbol{R} \mathrm{d}s \\
&+ \left[\mu \dot{\xi}^2 \eta^2(\xi) + N_\mathrm{P} \eta(\xi) - N(\xi) \eta(\xi) \right] \delta \xi \\
&+ \left[-(m_\mathrm{P} + \mu\xi) \boldsymbol{A}_\mathrm{P} - \mu \dot{\xi}^2 \frac{\partial \boldsymbol{R}(\xi)}{\partial s} + \boldsymbol{F}_\mathrm{P} + \boldsymbol{n}(\xi) \right] \delta \boldsymbol{R}_\mathrm{P} \\
&+ [-m_\mathrm{C} \boldsymbol{A}_\mathrm{C} + \boldsymbol{F}_\mathrm{C} - \boldsymbol{n}(L)] \delta \boldsymbol{R}_\mathrm{C} \equiv 0
\end{aligned} \tag{2.71}$$

Thus the equations of motion during retrieval are:

$$\begin{aligned}
G_R \triangleq &\int_\xi^L \left[-\mu \boldsymbol{A} + \frac{\partial \boldsymbol{n}}{\partial s} \right] \delta \boldsymbol{R} \mathrm{d}s \\
&+ \left[\mu \dot{\xi}^2 \eta(\xi)(\eta(\xi) - 1) + N_\mathrm{P} \eta(\xi) - N(\xi) \eta(\xi) \right] \delta \xi \\
&+ \left[-(m_\mathrm{P} + \mu\xi) \boldsymbol{A}_\mathrm{P} - \mu \dot{\xi}^2 \frac{\partial \boldsymbol{R}(\xi)}{\partial s} + \boldsymbol{F}_\mathrm{P} + \boldsymbol{n}(\xi) \right] \delta \boldsymbol{R}_\mathrm{P} \\
&+ [-m_\mathrm{C} \boldsymbol{A}_\mathrm{C} + \boldsymbol{F}_\mathrm{C} - \boldsymbol{n}(L)] \delta \boldsymbol{R}_\mathrm{C} \equiv 0
\end{aligned} \tag{2.72}$$

where, $\boldsymbol{A}$ denotes the accelerations caused by mechanomotive force except gravity force, which can be expressed as:

$$\boldsymbol{A} = \ddot{\boldsymbol{R}} + \mu \frac{GM}{|\boldsymbol{R}|^3} \boldsymbol{R} \tag{2.73}$$

$\boldsymbol{n}$ denotes the tension vector, which can be written as:

$$\boldsymbol{n} = N \boldsymbol{\tau} \tag{2.74}$$

The equations of motion of deployment and retrieval are similar due to Eq. (2.70) and Eq. (2.72). So in the following derivation, only deployment is considered.

Although Eq. (2.70) describes the deployment of operational robot, the orbit radium is contained in the vector $\boldsymbol{R}$, which is much larger than the relative orbit change caused by deployment. Solving Eq. (2.70) directly will lead to singular. The motion of the TSRS for space capture and maintenance is similar to the traditional rendezvous, which are described under the Hill coordinate (orbit coordinate). So Eq. (2.70) is rewritten under the orbit coordinate $oxyz$:

Vector $\boldsymbol{R}$ is:

$$\boldsymbol{R}(s,t) = \boldsymbol{R}_o(t) + \boldsymbol{r}(s,t) \tag{2.75}$$

where $\boldsymbol{R}_o$ is origin o of the orbit coordinate in the inertial coordinate. Since its motion is independent from the motion of the TSRS, we have:

$$\delta\boldsymbol{R} = \delta\boldsymbol{r} \tag{2.76}$$

$$\frac{\partial \boldsymbol{R}(s,t)}{\partial s} = \frac{\partial \boldsymbol{r}(s,t)}{\partial s}$$

In addition, according to the derivation of the Hill equation, we get:

$$\boldsymbol{A} = \begin{bmatrix} \ddot{x} - 2\omega\dot{z} \\ \ddot{y} + \omega^2 y \\ \ddot{z} + 2\omega\dot{x} - 3\omega^2 z \end{bmatrix} \tag{2.77}$$

where x, y, and z are the coordinates under the orbit coordinate system, and ω is the orbital velocity.

Substitute Eq. (2.76) and (2.77) into Eq. (2.70), the dynamics equations are:

$$\begin{aligned} G_D = & \int_{\xi}^{L} \left[-\mu\boldsymbol{A} + \frac{\partial \boldsymbol{n}}{\partial s} \right] \delta\boldsymbol{r} \mathrm{d}s \\ & + \left[\mu\dot{\xi}^2\eta^2(\xi) + N_{\mathrm{P}}\eta(\xi) - N(\xi)\eta(\xi) \right] \delta\xi \\ & + \left[-(m_{\mathrm{P}} + \mu\xi)\boldsymbol{A}_{\mathrm{P}} - \mu\dot{\xi}^2 \frac{\partial \boldsymbol{r}(\xi)}{\partial s} + \boldsymbol{F}_{\mathrm{P}} + \boldsymbol{n}(\xi) \right] \delta\boldsymbol{r}_{\mathrm{P}} \\ & + [-m_{\mathrm{C}}\boldsymbol{A}_{\mathrm{C}} + \boldsymbol{F}_{\mathrm{C}} - \boldsymbol{n}(L)]\delta\boldsymbol{r}_{\mathrm{C}} \equiv 0 \end{aligned} \tag{2.78}$$

Although Eq. (2.78) describes the motion completely, the integration range $[\xi(t), L]$ changes with the tether during deployment/retrieval.

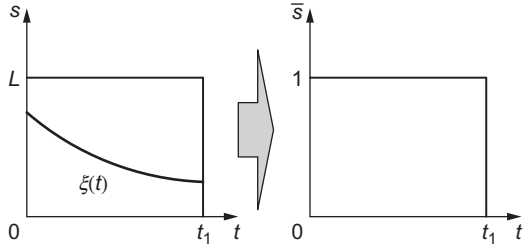

Fig. 2.22 Transformation of integrating range.

The traditional finite-element method is not useful anymore. To solve this question, we change the integration range into [0,1] as shown in Fig. 2.22. With this method, the consistency of the integration range is ensured; and it is easy for discretization.

A nondimensional variable $\bar{s}$ is introduced and defined as:

$$\bar{s}=\frac{1}{l}(s-\xi) \tag{2.79}$$

where l is the released length of the tether, defined as $l=L-\xi$. Additionally, it is used to describe the position vector of $\bar{s}$, thus we get:

$$\begin{cases} \dfrac{\partial \boldsymbol{r}}{\partial s}=\dfrac{1}{l}\overline{\boldsymbol{r}}' \\ \dfrac{\partial \boldsymbol{r}}{\partial t}=\dot{\overline{\boldsymbol{r}}}+\overline{\boldsymbol{r}}'(1-\bar{s})\dfrac{\dot{l}}{l} \\ \dfrac{\partial^2 \boldsymbol{r}}{\partial s^2}=\dfrac{1}{l^2}\overline{\boldsymbol{r}}'' \\ \dfrac{\partial^2 \boldsymbol{r}}{\partial t^2}=\ddot{\overline{\boldsymbol{r}}}+2(1-\bar{s})\dfrac{\dot{l}}{l}\dot{\overline{\boldsymbol{r}}}'+(1-\bar{s})^2\dfrac{\dot{l}^2}{l^2}\overline{\boldsymbol{r}}'' \\ \qquad\qquad +(1-\bar{s})\dfrac{\ddot{l}}{l}\overline{\boldsymbol{r}}'-(1-\bar{s})\dfrac{2\dot{l}^2}{l^2}\overline{\boldsymbol{r}}' \end{cases} \tag{2.80}$$

Substitute Eq. (2.80) into Eq. (2.78):

$$\begin{aligned} G_D=&\int_0^1\left(-\mu l\overline{\boldsymbol{A}}\delta\overline{\boldsymbol{r}}-\overline{\boldsymbol{n}}\cdot\delta\overline{\boldsymbol{r}}'\right)\mathrm{d}s \\ &+\left[\mu\dot{\xi}^2\overline{\eta}^2(0)+N_{\mathrm{P}}\overline{\eta}(0)-\overline{N}(0)\overline{\eta}(0)\right]\delta\xi \\ &+\left[-(m_{\mathrm{P}}+\mu\xi)\boldsymbol{A}_{\mathrm{P}}-\mu\dot{\xi}^2\overline{\eta}(0)\boldsymbol{\tau}(0)+\boldsymbol{F}_{\mathrm{P}}\right]\delta\overline{\boldsymbol{r}}(0) \\ &+\left[-m_{\mathrm{C}}\boldsymbol{A}_{\mathrm{C}}+\boldsymbol{F}_{\mathrm{C}}\right]\delta\overline{\boldsymbol{r}}(1)\equiv 0 \end{aligned} \tag{2.81}$$

where:

$$\bar{\eta}=\frac{1}{l}|r'|$$

$$\bar{A}=\begin{bmatrix} \ddot{\bar{x}}+2(1-\bar{s})\frac{\dot{l}}{l}\dot{\bar{x}}'+(1-\bar{s})^2\frac{\dot{l}^2}{l^2}\bar{x}''+(1-\bar{s})\frac{\ddot{l}}{l}\bar{x}'-2(1-\bar{s})\frac{\dot{l}^2}{l^2}\bar{x}'-2\omega\left[\dot{\bar{z}}+\frac{\dot{l}}{l}(1-\bar{s})\bar{z}'\right] \\ \ddot{\bar{y}}+2(1-\bar{s})\frac{\dot{l}}{l}\dot{\bar{y}}'+(1-\bar{s})^2\frac{\dot{l}^2}{l^2}\bar{y}''+(1-\bar{s})\frac{\ddot{l}}{l}\bar{y}'-2(1-\bar{s})\frac{\dot{l}^2}{l^2}\bar{y}'+\omega^2\bar{y} \\ \ddot{\bar{z}}+2(1-\bar{s})\frac{\dot{l}}{l}\dot{\bar{z}}'+(1-\bar{s})^2\frac{\dot{l}^2}{l^2}\bar{z}''+(1-\bar{s})\frac{\ddot{l}}{l}\bar{z}'-2(1-\bar{s})\frac{\dot{l}^2}{l^2}\bar{z}'+2\omega\left[\dot{\bar{x}}+\frac{\dot{l}}{l}(1-\bar{s})\bar{x}'\right]-3\omega^2\bar{z} \end{bmatrix}$$

$$\bar{n}=\frac{1}{2}EA\left\{\left(\frac{|\bar{r}'|}{l}-1-\varepsilon_0\right)+\sqrt{\left(\frac{|\bar{r}'|}{l}-1-\varepsilon_0\right)^2+4\left(\frac{T_0}{EA}\right)^2}+2\frac{\alpha}{l}\left[\frac{\bar{r}'\cdot\dot{\bar{r}}'}{|\bar{r}'|}-(\bar{s}-1)\frac{\dot{l}}{l}\frac{\bar{r}'\cdot\bar{r}''}{|\bar{r}'|}-\frac{\dot{l}}{l}|\bar{r}'|\right]\right\}\frac{\bar{r}'}{|\bar{r}'|}$$

To solve the motion of the system, discretization of integration terms in Eq. (2.81) is required. Because the finite element method is more precise compared to the Bead model and the Ritz method, we use the finite element method in this section for discretization of the dynamics equations.

Interval [0,1] is divided into n segments by $n+1$ nodes. A three-order interpolation function is used in each segment as shown in Fig. 2.23. Thus the interpolation function for ith segment is expressed as:

$$\begin{cases} \varphi_{i1}=2n^3\bar{s}^3-(6i-3)n^2\bar{s}^2+6i(i-1)n\bar{s}-i^2(2i-3) \\ \varphi_{i2}=\frac{1}{n}\left[n^3\bar{s}^3-(3i-1)n^2\bar{s}^2+i(3i-2)n\bar{s}-i^2(i-1)\right] \\ \varphi_{i3}=-2n^3\bar{s}^3+(6i-3)n^2\bar{s}^2-6i(i-1)n\bar{s}+(2i+1)(i-1)^2 \\ \varphi_{i4}=\frac{1}{n}\left[n^3\bar{s}^3-(3i-2)n^2\bar{s}^2+(3i-1)(i-1)n\bar{s}-i(i-1)^2\right] \end{cases} \quad \left(\frac{i-1}{n}\le s\le\frac{i}{n}\right) \tag{2.82}$$

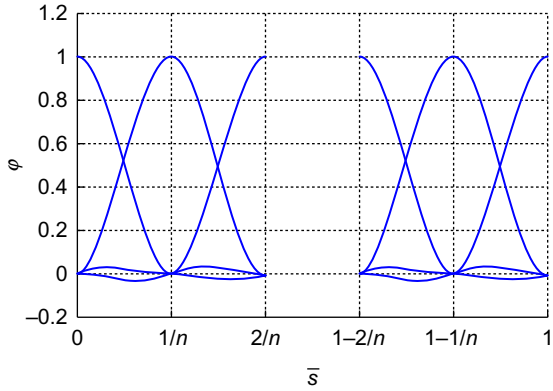

Fig. 2.23 Interpolation function.

The position vector of ith segment is:

$$\boldsymbol{r} \approx \begin{bmatrix} \varphi_{i1} & \varphi_{i2} & \varphi_{i3} & \varphi_{i4} \end{bmatrix} \begin{bmatrix} \overline{\boldsymbol{r}}_i \\ \overline{\boldsymbol{r}'}_i \\ \overline{\boldsymbol{r}'}_{i+1} \\ \overline{\boldsymbol{r}'}_{i+1} \end{bmatrix} \tag{2.83}$$

Integrate the acceleration of ith segment, we get:

$$\int_{(i-1)/n}^{i/n} \overline{\boldsymbol{A}} \delta \overline{\boldsymbol{r}} \mathrm{d}s \approx \delta \boldsymbol{u}_i^{\mathrm{T}} \left(\boldsymbol{M}_i \ddot{\boldsymbol{u}}_i + \boldsymbol{C}_i \dot{\boldsymbol{u}}_i + \boldsymbol{K}_i \boldsymbol{u}_i \right) \tag{2.84}$$

where:

$$\boldsymbol{u}_i = \left[\overline{x}_i, \overline{x}_{i+1}, \overline{y}_i, \overline{y}_{i+1}, \overline{z}_i, \overline{z}_{i+1} \right]^{\mathrm{T}} \tag{2.85}$$

$$\boldsymbol{M}_i = \begin{bmatrix} \boldsymbol{M}_{\varphi\varphi}^{(i)} & & \\ & \boldsymbol{M}_{\varphi\varphi}^{(i)} & \\ & & \boldsymbol{M}_{\varphi\varphi}^{(i)} \end{bmatrix} \tag{2.86}$$

$$\boldsymbol{C}_i = \begin{bmatrix} 2\frac{\dot{l}}{l}\boldsymbol{M}_{\varphi\varphi'}^{(i)} & & -2\omega\boldsymbol{M}_{\varphi\varphi}^{(i)} \\ & 2\frac{\dot{l}}{l}\boldsymbol{M}_{\varphi\varphi'}^{(i)} & \\ 2\omega\boldsymbol{M}_{\varphi\varphi}^{(i)} & & 2\frac{\dot{l}}{l}\boldsymbol{M}_{\varphi\varphi'}^{(i)} \end{bmatrix} \tag{2.87}$$

$$\boldsymbol{K}_i = \begin{bmatrix} \boldsymbol{M}_K^{(i)} & & -2\omega\frac{\dot{l}}{l}\boldsymbol{M}_{\varphi\varphi'}^{(i)} \\ & \boldsymbol{M}_K^{(i)} + \omega^2\boldsymbol{M}_{\varphi\varphi}^{(i)} & \\ -2\omega\frac{\dot{l}}{l}\boldsymbol{M}_{\varphi\varphi'}^{(i)} & & \boldsymbol{M}_K^{(i)} - 3\omega^2\boldsymbol{M}_{\varphi\varphi}^{(i)} \end{bmatrix} \tag{2.88}$$

where:

$$\boldsymbol{M}_K^{(i)} = \frac{\dot{l}^2}{l^2}\boldsymbol{M}_{\varphi\varphi''}^{(i)} + \left(\frac{\ddot{l}}{l} - 2\frac{\dot{l}^2}{l^2} \right) \boldsymbol{M}_{\varphi\varphi'}^{(i)} \tag{2.89}$$

$$\boldsymbol{M}_{\varphi\varphi}^{(i)}(j,k) = \int_{(i-1)/n}^{i/n} \varphi_{ij}\varphi_{ik}\mathrm{d}\overline{s} \tag{2.90}$$

$$\boldsymbol{M}_{\varphi\varphi'}^{(i)}(j,k)=\int_{(i-1)/n}^{i/n}(1-\bar{s})\varphi_{ij}\varphi'_{ik}\mathrm{d}\bar{s} \tag{2.91}$$

$$\boldsymbol{M}_{\varphi\varphi''}^{(i)}(j,k)=\int_{(i-1)/n}^{i/n}(1-\bar{s})^2\varphi_{ij}\varphi''_{ik}\mathrm{d}\bar{s} \tag{2.92}$$

The stress integration of ith segment is:

$$\int_{(i-1)/n}^{i/n}\overline{\boldsymbol{n}}\cdot\delta\overline{\boldsymbol{r}}'\mathrm{d}s\approx\delta\boldsymbol{u}_i^{\mathrm{T}}\boldsymbol{R}_i=\delta\boldsymbol{u}_i^{\mathrm{T}}\int_{(i-1)/n}^{i/n}\begin{bmatrix}\boldsymbol{\Phi}_i & & \\ & \boldsymbol{\Phi}_i & \\ & & \boldsymbol{\Phi}_i\end{bmatrix}\begin{bmatrix}\overline{n}_x\\ \overline{n}_y\\ \overline{n}_z\end{bmatrix}\mathrm{d}s \tag{2.93}$$

where:

$$\boldsymbol{\Phi}_i=[\varphi_{i1},\varphi_{i2},\varphi_{i3},\varphi_{i4}]^{\mathrm{T}} \tag{2.94}$$

In the real calculation, the five-order Gauss numerical integration method is used to solve integration terms in Eq. (2.93).

The whole position vector is:

$$\boldsymbol{U}=[\overline{x}_1,\cdots,\overline{x}_{n+1},\overline{y}_1,\cdots,\overline{y}_{n+1},\overline{z}_1,\cdots,\overline{z}_{n+1}]^{\mathrm{T}} \tag{2.95}$$

Matrix $\boldsymbol{M}_i$, $\boldsymbol{C}_i$ and $\boldsymbol{K}_i$ are assembled as shown in Fig. 2.24. The total matrix are $\boldsymbol{M}$, $\boldsymbol{C}$, and $\boldsymbol{K}$ respectively. The total stress vector $\boldsymbol{R}$ is acquired via similar assembly. Substitute the total matrix into Eq. (2.81), we get:

$$\begin{aligned}G_D\approx\delta\boldsymbol{U}^{\mathrm{T}}&\left[-\mu l\left(\boldsymbol{M}\ddot{\boldsymbol{U}}+\boldsymbol{C}\dot{\boldsymbol{U}}+\boldsymbol{K}\boldsymbol{U}\right)-\boldsymbol{R}\right]\\&+\left[\mu\dot{\xi}^2\overline{\eta}^2(0)+N_{\mathrm{P}}\overline{\eta}(0)-\overline{N}(0)\overline{\eta}(0)\right]\delta\xi\\&+\left[-(m_{\mathrm{P}}+\mu\xi)\boldsymbol{A}_{\mathrm{P}}-\mu\dot{\xi}^2\overline{\eta}(0)\boldsymbol{\tau}(0)+\boldsymbol{F}_{\mathrm{P}}\right]\delta\overline{\boldsymbol{r}}(0)\\&+[-m_{\mathrm{C}}\boldsymbol{A}_{\mathrm{C}}+\boldsymbol{F}_{\mathrm{C}}]\delta\overline{\boldsymbol{r}}(1)\equiv 0\end{aligned} \tag{2.96}$$

where:

$$\begin{aligned}\delta\overline{\boldsymbol{r}}(0)&=[\delta\boldsymbol{U}(1),\delta\boldsymbol{U}(2n+3),\delta\boldsymbol{U}(4n+5)]^{\mathrm{T}}\\\delta\overline{\boldsymbol{r}}(0)&=[\delta\boldsymbol{U}(2n+1),\delta\boldsymbol{U}(4n+3),\delta\boldsymbol{U}(6n+5)]^{\mathrm{T}}\end{aligned}$$

After consolidating like terms, we get:

$$\begin{aligned}G_D\approx\delta\boldsymbol{U}^{\mathrm{T}}&\left[-\left(\hat{\boldsymbol{M}}\ddot{\boldsymbol{U}}+\hat{\boldsymbol{C}}\dot{\boldsymbol{U}}+\hat{\boldsymbol{K}}\boldsymbol{U}+\boldsymbol{R}\right)+\boldsymbol{F}\right]\\&+\left[\mu\dot{\xi}^2\overline{\eta}^2(0)+N_{\mathrm{P}}\overline{\eta}(0)-\overline{N}(0)\overline{\eta}(0)\right]\delta\xi\equiv 0\end{aligned} \tag{2.97}$$

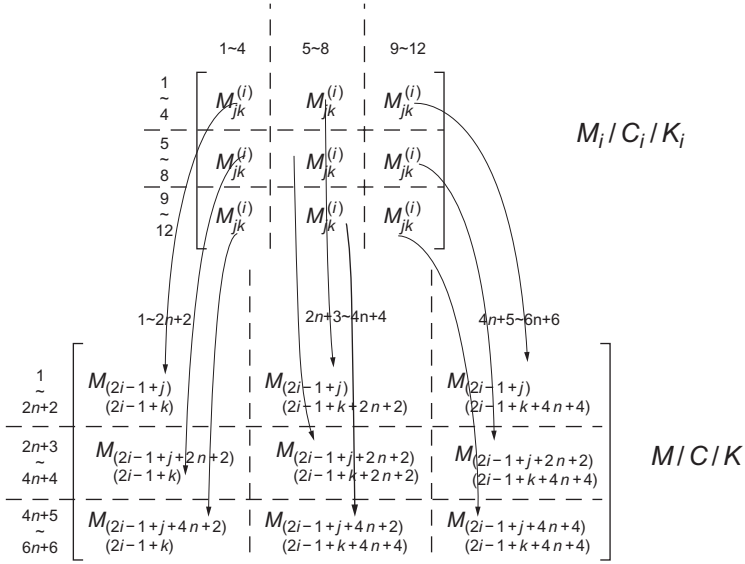

Fig. 2.24 Schematic of assembly process.

where $\hat{\boldsymbol{M}}$ is the equivalent mass matrix of the system, $\hat{C}$ is the equivalent damping matrix of the system, $\hat{\boldsymbol{K}}$ is the equivalent stiffness matrix of the system, $\boldsymbol{F}$ is the equivalent mechanomotive force matrix of the system. The detailed calculations are shown in appendix. Eq. (2.97) is equivalence to:

$$\boldsymbol{P}\left(t, \hat{\boldsymbol{U}}, \dot{\hat{\boldsymbol{U}}}, \ddot{\hat{\boldsymbol{U}}}\right) = \begin{bmatrix} \boldsymbol{F} - \left(\hat{\boldsymbol{M}}\ddot{\boldsymbol{U}} + \hat{\boldsymbol{C}}\dot{\boldsymbol{U}} + \hat{\boldsymbol{K}}\boldsymbol{U} + \boldsymbol{R}\right) \\ \mu\dot{\xi}^2\overline{\eta}^2(0) + \mathrm{N_P}\overline{\eta}(0) - \overline{N}(0)\overline{\eta}(0) \end{bmatrix} = 0 \tag{2.98}$$

where $\hat{\boldsymbol{U}} = \left[\boldsymbol{U}^{\mathrm{T}}, \xi\right]^{\mathrm{T}}$.

Because Eq. (2.98) is a set of implicit differential equations, nonlinear iteration is required for solving it. To ensure the high efficiency and large domain of convergence, we use the Newton-Raphson method to correct the time domain by iteration.

The discrete time step is h. The states at t moment is used to predict the states at $t+h$, which is written as:

$$\begin{cases} \ddot{\hat{\boldsymbol{U}}}^{(0)}(t+h) = \ddot{\hat{\boldsymbol{U}}}(t) \\ \dot{\hat{\boldsymbol{U}}}^{(0)}(t+h) = \dot{\hat{\boldsymbol{U}}}(t) + h\left[(1-\gamma)\ddot{\hat{\boldsymbol{U}}}(t) + \gamma\ddot{\hat{\boldsymbol{U}}}(t+h)\right] \\ \hat{\boldsymbol{U}}^{(0)}(t+h) = \hat{\boldsymbol{U}}(t) + h\dot{\hat{\boldsymbol{U}}}(t) + h^2\left[(0.5-\beta)\ddot{\hat{\boldsymbol{U}}}(t) + \beta\ddot{\hat{\boldsymbol{U}}}(t+h)\right] \end{cases} \tag{2.99}$$

where the detailed derivation of parameters γ and β are shown in the references respectively.

The variation of Eq. (2.98) is:

$$\delta \boldsymbol{P} = \frac{\partial \boldsymbol{P}}{\partial \hat{\boldsymbol{U}}}\delta \hat{\boldsymbol{U}} + \frac{\partial \boldsymbol{P}}{\partial \dot{\hat{\boldsymbol{U}}}}\delta \dot{\hat{\boldsymbol{U}}} + \frac{\partial \boldsymbol{P}}{\partial \ddot{\hat{\boldsymbol{U}}}}\delta \ddot{\hat{\boldsymbol{U}}} \tag{2.100}$$

According to Eq. (2.99), the states at $t+h$ moment are:

$$\begin{cases} \delta \dot{\hat{\boldsymbol{U}}} = \dfrac{\gamma}{h\beta}\delta \hat{\boldsymbol{U}} \\ \delta \ddot{\hat{\boldsymbol{U}}} = \dfrac{1}{h^2\beta}\delta \hat{\boldsymbol{U}} \end{cases} \tag{2.101}$$

Thus:

$$\delta \boldsymbol{P} = \left(\frac{\partial \boldsymbol{P}}{\partial \hat{\boldsymbol{U}}} + \frac{\gamma}{h\beta}\frac{\partial \boldsymbol{P}}{\partial \dot{\hat{\boldsymbol{U}}}} + \frac{1}{h^2\beta}\frac{\partial \boldsymbol{P}}{\partial \ddot{\hat{\boldsymbol{U}}}} \right)\delta \hat{\boldsymbol{U}} \tag{2.102}$$

The predictive value acquired from Eq. (2.99) is the initial of iteration, and then the iteration revision is shown as:

$$\begin{cases} \Delta \hat{\boldsymbol{U}}^{(i)} = -\left(\dfrac{\partial \boldsymbol{P}^{(i)}}{\partial \hat{\boldsymbol{U}}} + \dfrac{\gamma}{h\beta}\dfrac{\partial \boldsymbol{P}^{(i)}}{\partial \dot{\hat{\boldsymbol{U}}}} + \dfrac{1}{h^2\beta}\dfrac{\partial \boldsymbol{P}^{(i)}}{\partial \ddot{\hat{\boldsymbol{U}}}} \right)^{-1} \boldsymbol{P}^{(i)} \\ \hat{\boldsymbol{U}}^{(i+1)} = \hat{\boldsymbol{U}}^{(i)} + \Delta \hat{\boldsymbol{U}}^{(i)} \\ \dot{\hat{\boldsymbol{U}}}^{(i+1)} = \dot{\hat{\boldsymbol{U}}}^{(i)} + \dfrac{\gamma}{h\beta}\Delta \hat{\boldsymbol{U}}^{(i)} \\ \ddot{\hat{\boldsymbol{U}}}^{(i+1)} = \ddot{\hat{\boldsymbol{U}}}^{(i)} + \dfrac{1}{h^2\beta}\Delta \hat{\boldsymbol{U}}^{(i)} \end{cases} \tag{2.103}$$

when $\left\| \boldsymbol{P}^{(i)}(t+h) \right\|_2 \leq P_T$, iteration stops, and $\hat{U}^{(i)}$ is taken as the true value at $t+h$ approximately.

REFERENCES

[1] A.K. Misra, V.J. Modi, Dynamics and control of tether connected two-body systems-a brief review, in: vol. 1, 1982.

[2] P.K. Lakshmanan, V.J. Modi, A.K. Misra, Dynamics and control of the tethered satellite system in the presence of offsets, Acta Astronaut. 15 (12) (1987) 1053–1057.

[3] P. Williams, In-plane payload capture with an elastic tether, J. Guid. Control. Dyn. 29 (4) (2006) 810–821.

[4] P. Williams, Optimal deployment/retrieval of tethered satellites, J. Spacecr. Rocket. 45 (2) (2008) 324–343.

[5] P. Williams, et al., In-plane payload capture using tethers, Acta Astronaut. 57 (10) (2005) 772–787.

[6] T.S. No, J.E. Cochran Jr., Dynamics and control of a tethered flight vehicle, J. Guid. Control. Dyn. 18 (1) (1995) 66–72.
[7] A.K. Banerjee, Dynamics of tethered payloads with deployment rate control, J. Guid. Control. Dyn. 13 (4) (1990) 759–762.
[8] A.N. Danilin, et al., Dynamics of a space vehicle with elastic deploying tether, Comput. Struct. 72 (1) (1999) 141–147.
[9] B.S. Yu, D.P. Jin, Deployment and retrieval of tethered satellite system under J 2 perturbation and heating effect, Acta Astronaut. 67 (7) (2010) 845–853.
[10] K.K. Mankala, S.K. Agrawal, Dynamic modeling and simulation of satellite tethered systems, J. Vib. Acoust. 127 (2) (2005) 144–156.
[11] K.K. Mankala, S.K. Agrawal, Dynamic modeling and simulation of impact in tether net/gripper systems, Multibody Sys. Dyn. 11 (3) (2004) 235–250.
[12] K.K. Mankala, S.K. Agrawal, Dynamic modeling of satellite tether systems using Newton's laws and Hamilton's principle, J. Vib. Acoust. 130 (1) (2008)014501.
[13] K.K. Mankala, Satellite tether systems: dynamic modeling and control, PhD Dissertation, University of Delaware, Newark, USA, 2006.
[14] E.B. Crellin, et al., On balance and variational formulations of the equation of motion of a body deploying along a cable, J. Appl. Mech. 64 (2) (1997) 369–374.
[15] M. Krupa, et al., Modeling, dynamics and control of tethered satellite systems, Nonlinear Dyn. 43 (1–2) (2006) 73–96.
[16] J.L. Tang, et al., Dynamics of variable-length tethers with application to tethered satellite deployment, Commun. Nonlinear Sci. Numer. Simul. 16 (8) (2011) 3411–3424.
[17] B. Bischof, et al., ROGER—Robotic geostationary orbit restorer, Sci. Technol. Ser. 109 (2004) 183–193.
[18] S.A. Crist, J.G. Eisley, Cable motion of a spinning spring-mass system in orbit, J. Spacecr. Rocket. 7 (11) (1970) 1352–1357.
[19] D.L. Akin, M.L. Bowden, SCOUT: EVA capabilities of the space construction and orbital utility transport. no. 2004-01-2295. SAE Technical Paper, 2004.

FURTHER READING

[20] R. Orban, Advances in space tether materials, in: 3rd International Conference on Tethers in Space-Toward Flight, San Francisco, CA, 1989.